American Mineralogist, Volume 92, pages 1502–1517, 2007

Temperature dependence of IR absorption of hydrous/hydroxyl species in minerals and synthetic materials

Ming Zhang,[1,*] Ekhard K.H. Salje,[1] Michael A. Carpenter,[1] Ji Yang Wang,[2] Lee A. Groat,[3] George A. Lager,[4] Ling Wang,[5] Anton Beran,[6] and Ulrich Bismayer[7]

[1]Department of Earth Sciences, University of Cambridge, Downing Street, Cambridge, CB2 3EQ, U.K.
[2]National Laboratory of Crystal Material, Institute of Crystal Material, Shandong University, Jinan 250100, Shandong, P.R. China
[3]Department of Earth and Ocean Sciences, University of British Columbia, Vancouver, British Columbia, V6T 1Z4, Canada
[4]Department of Geography and Geosciences, University of Louisville, Louisville, Kentucky, U.S.A.
[5]College of Materials and Chemistry and Chemical Engineering, Chengdu University of Technology, Chengdu 610059, Sichuan, P.R. China
[6]Institut für Mineralogie und Kristallographie, Universität Wien—Geozentrum, Althanstrasse 14, A-1090 Wien, Austria
[7]Mineralogisch-Petrographisches Institut, Universität Hamburg, Grindelallee 48, D-20146 Hamburg, Germany

Abstract

We report on temperature dependencies of infrared (IR) fundamental, combination, and overtone vibrations of hydroxyl species (OH) in nominally anhydrous minerals (e.g., titanite), ferroelectric crystals ($KTa_{1-x}Nb_xO_3$, KTN), layer silicates (talc, mica, and pyrophyllite), and hydrous minerals such as apatite and synthetic hydrous/deuterated garnets [$Ca_3Al_2(O_4H_4)_3$ and $Ca_3Al_2(O_4D_4)_3$] for the temperature range of 20–300 K. Data obtained by high-resolution FTIR spectroscopy show that increasing temperature generally leads to a decrease in the band height and band area of fundamental vibrations of hydroxyl species, whereas the combination and first-overtone bands commonly show different temperature dependencies. The results show that in the investigated temperature range, the variations of the band height and area for different OH bands (especially for combinations and overtones) on cooling or heating do not reflect changes in OH concentrations in the materials, but relate to temperature-dependent absorption coefficients. The observations imply that absorption coefficients calibrated at room temperature cannot necessarily be used for the determination of hydroxyl contents at other temperatures.

Keywords: Infrared spectroscopy, low temperature, apatite, hydrous garnet, pyrophyllite, talc, sericite, titanite

Introduction

Hydrous and hydroxyl species in minerals, melts, glasses, and synthetic materials have been the subject of extensive studies. Water molecules, hydroxide ions, and fluid inclusions are important components of many natural systems and are also prominent in a variety of synthetic minerals and technological materials. The presence of hydrous species may affect the physical properties of minerals and synthetic materials. Traces of OH in nominally anhydrous minerals are capable of recycling water from the hydrosphere back into the mantle. Analysis of these hydrous species can reveal important information on the crystal chemistry, local structural modifications, and atomic order-disorder processes in minerals and crystals, and may lead to new information on the stability of hydrous phases, thermal or hydrothermal history, and geologic environments of the host rocks of the minerals. A better understanding of the incorporation mechanism of hydrous species in silicate glasses and melts may yield insight into kinetic processes during magma degassing and for modeling thermodynamic properties of magmas. Determinations of the frozen-in hydrous speciation in natural mineral glasses may offer information on the cooling rate of the host rocks. The hydrogen content of minerals may be used to extract information on water or oxygen fugacity and silica activity related to metamorphic and metasomatism events (e.g., Langer et al. 1993; Zhang et al. 2003).

As one of the most sensitive techniques for detecting and analyzing hydrous/hydroxyl species, IR spectroscopy has been widely used for investigations of hydrous components, "water" concentrations, and their locations in crystal structures (e.g., Nakamoto et al. 1955; Novak 1974; Paterson 1982; Stolper 1982; Aines and Rossman 1984, 1985; Hemley et al. 1987; Rossman 1988; McMillan 1995; Libowitzky and Rossman 1997; Struzhkin et al. 1997; Hofmeister et al. 1999; Zhang et al. 2001; Johnson and Rossman 2003; Libowitzky and Beran 2004), as well as hydrous speciation, solubility, and kinetics of reactions in glasses and melts (Keppler and Bagdassarov 1993; Zhang et al. 1995; Nowak and Behrens 1995; Shen and Keppler 1995; Behrens et al. 1996; Carroll and Blank 1997; Ihinger et al. 1999; Withers and Behrens 1999; Sowerby and Keppler 1999; Zhang, Y. et al. 2000; Okumura et al. 2003; Liu et al. 2004; Okumura and Nakashima 2005).

* E-mail: mz10001@esc.cam.ac.uk

0003-004X/07/0809–1502$05.00/DOI: 10.2138/am.2007.2586

Our attention was initially drawn to this topic by our recent experimental results for crystalline and metamict titanite (Salje et al. 2000; Zhang, M. et al. 2000, 2001). These studies have shown that the temperature dependencies of OH bands obtained from in situ IR experiments are significantly different from those obtained from quench experiments, even taking into account different heating rates and annealing times. A systematic decrease of integral absorbance for hydroxyl bands of titanite appeared at temperatures of 400–500 K during in situ heating measurements, whereas in quench experiments a significant loss of "water" did not take place until the samples were annealed above 800 K. Although the formation of new OH bands and conversions between and among different species (e.g., OH and H_2O) might cause the differences, experimental data do not favor this explanation because observations from crystalline titanite in both in situ and quenched experiments failed to show the development of extra hydrous features. This led us to wonder whether the different temperature evolutions observed from quench and in-situ experiments have the same physical origins, whether it is simply due to temperature-induced changes of absorption intensity and coefficients or changes of dipole moments, and to what extent and under what conditions conversions between species can take place. The present study was also driven by the fact that in-situ IR spectroscopy has commonly been employed to study hydrous and hydroxyl species, their concentrations, and reaction processes at different temperatures. Moreover, their multiphonon bands have often been used for the quantitative analysis of the "water" content. There is apparently a lack of good understanding of the possible temperature dependence of IR bands, which could affect or hinder applications based on the Beer-Lambert law in concentration determinations and may complicate data analysis. There appears also to be confusion about the origins or causes of the possible change of hydrous band intensities with temperatures, especially for multiphonon bands involving OH.

The goals of the present study were to gain an understanding of the extent to which absorption intensity may be affected by temperature, to clarify whether OH multiphonon bands have temperature dependencies essentially similar to or different from their OH fundamentals, and to gain a better insight into validation of Beer-Lambert law. In this study, we were mainly interested in examining the relative change of absorption between room temperature and low temperatures. In the first part of the project, the temperature evolution of MIR and NIR spectra of minerals and clays was investigated and the experimental data are presented here. Studies of hydrous species in glasses and disordered materials and the effect of pressure on the species will be published separately. As maintaining constant concentrations of OH species during measurements is the key factor for a successful study of temperature dependence of absorption coefficient, layer silicates (pyrophyllite, talc, and mica), nominally anhydrous minerals or materials (titanite and $KTa_{1-x}Nb_xO_3$, KTN), and hydrous minerals (hydrous/deuterated garnet and apatite) were examined at low temperatures (20–300 K). This was done to avoid or to minimize possible temperature-induced proton migration, which is expected to be more active at high temperatures (e.g., above 500 or 600 K), and also to prevent the possible loss of hydrogen (e.g., partial dehydroxylation or dehydration caused by heating to high temperature), which may lead to irreversible decreases in hydroxyl and hydrous concentrations, and will undoubtedly cause changes in the related IR absorptions. The measurements at low temperatures are also expected to reduce the possible surface absorption, which is expected to be more significant at high temperature and to be less temperature dependent at low temperatures (Rowe and Harrington 1976). In this paper, we focus on contributions related to temperature on absorption coefficient, and eliminate or minimize the possible absorption changes caused by variations of hydroxyl or hydrous concentrations in the samples at high temperatures. Moreover, the data from low-temperature measurements may offer a good indication or estimation of the possible degree of change related to absorption intensity at high temperatures because single-phonon and multiphonon bands are expected to follow certain behaviors over large temperature ranges (see subsequent sections). An additional aim of this study was to investigate the vibrational characteristics of hydrous bands, as more bands can be observed at low temperatures due to band sharpening.

Concepts of infrared absorption

To clarify the notation in this paper, we briefly repeat some fundamentals of infrared absorption. The infrared absorption intensity of a crystal is expressed in terms of an absorption coefficient A (in cm^{-1}) that is defined by:

$$I = I_0 e^{-Al} \text{ or } A = \frac{1}{l}\log(\frac{I_0}{I}) \quad (1)$$

where I_0 is the incident radiation energy at a given frequency or wavenumber, I is the transmitted energy, and l (in cm) is the sample thickness. For a band of vibrations consisting of several modes, the absorption is better described by:

$$A' = \int_{band} A d\omega \quad (2)$$

where ω is frequency (usually expressed in wavenumbers) and the integral is over the limits of the absorption band and gives the integrated absorption intensity of the band. It has been well recognized (e.g., Schnepp 1967; Bolkenhtein et al. 1972; Sherwood 1972; Decius and Hexter 1977; Hollas 1996) that absorption intensity of the infrared mode is related to the transition matrix element of the dipole moment:

$$\int \psi_f^* \mu \, \psi_l d\tau \quad (3)$$

where μ is the instantaneous dipole moment of the vibrational transition along the direction of polarization of the incident radiation, ψ_f is the wave function for the initial state involved in the transition (the ground state), and ψ_l is the wave function for the final state involved in the transition (the excited state). Both ψ_f and ψ_l are functions of the normal coordinates and depend on the symmetries of the normal mode vibrations in the initial and existed states. For a vibrational transition, the integral in Equation 3 must be non-zero so that a transition may be allowed. This requirement also gives the selection rules (e.g., Birman 1963; Davydov 1976) which define the activity of infrared modes.

Dipole moment, μ, can be expressed as a series in terms of Q_i, the normal coordinates that describe the atomic and molecular displacements (e.g., Thomas et al. 1971):

$$\mu = \mu_0 + \sum_i \left(\frac{\partial \mu}{\partial Q_i}\right) Q_i + \frac{1}{2}\sum_{ij}\left(\frac{\partial^2 \mu}{\partial Q_i \partial Q_j}\right) Q_i Q_j + ... \quad (4)$$

where μ_0 is the permanent dipole moment, which is a constant and does not contribute to the integral in Equation 3 since:

$$\int \psi_f^* \psi_l d\tau = 0 . \quad (5)$$

The linear or harmonic term in Equation 4 contributes to single-phonon absorption, whereas the higher-order terms in Equation 4, or anharmonic terms in the potential energy and/or a non-linear dielectric nature, are understood to be responsible for multiphonon processes (i.e., one photo interacts with multiphonons simultaneously) (Lax and Burstein 1955; Kleinman 1960; Born and Huang 1968; Nedoluha 1970; Bendow et al. 1974; Sparks 1974; Thibaudeau et al. 2006). Theoretically, absorptions of phonon processes are dominated by three factors: the oscillator strength of the transitions involving one photon and a set of *n* phonons, the density state of these phonons, and the respective phonon occupancies (Mills and Maradudin 1973; Bendow 1973; Bendow et al. 1973; Sparks and Sham 1973b; Piccirillo et al. 2002). Under harmonic approximation, the integral in Equation 3 can be rewritten as:

$$\int \psi_f^* \mu \ \psi_l d\tau = \left(\int \psi_f^* Q_i \psi_l dQ_i\right)\left(\frac{\partial \mu}{\partial Q_i}\right) . \quad (6)$$

Therefore, the transition moment described by Equation 3 is mainly determined by the linear term in Equation 4 and is proportional to dipole moment derivative, $\partial\mu/\partial Q_i$. As absorption intensities are proportional to the square of the magnitude of the transition dipole moment, therefore, with harmonic approximation,

$$A_i \propto \left(\frac{\partial \mu}{\partial Q_i}\right)^2 \quad (7)$$

that is, absorption intensity is proportional to the square of the change of dipole moments. The change of dipole moment, $\partial\mu/\partial Q_i$, can be connected to several factors, such as the permanent dipole moment in molecules or ions in a crystal, the dipole moment induced by neighboring molecular quadrupole and dipole moments, and the dipole moment caused by short-range forces that cause distortion of the electronic cloud (Schnepp 1967; van Straten and Smit 1976). The values of $(\partial\mu/\partial Q_i)$ for some materials are extracted from infrared absorption intensity (e.g., Davies and Orville-Thomas 1969; Thomas et al. 1969, 1971; Galabov and Orville-Thomas 1973; Stoeckli-Evavs et al. 1975).

Experimentally, a more commonly used form of absorption intensity is given by the Beer-Lambert law (Pfeiffer and Liebhafsky 1951; Malinin and Yoe 1961):

$$I = I_0 e^{-\mathrm{Al}} = I_0 e^{-\mathrm{acl}} \text{ or } A = \log\left(\frac{I_0}{I}\right) = \mathrm{acl} . \quad (8)$$

The law asserts that the absorption intensity or integrated absorption intensity of a species or phase in the measured sample is directly proportional to the concentration *c* (in mol/L) of the species and path length or thickness (in cm) of the sample. The constant of proportionality, *a*, is referred as the molar absorption coefficient [in L/(mol·cm)] or integral molar absorption coefficient [in L/(mol·cm^2)], which can be determined experimentally. For hydrous and hydroxyl species, the concentration (in mol/L) of the species can be expressed in wt% H_2O by multiplying by a factor of $1.8/D$ (where *D* is the density in g/cm^3). The concentrations of different species can be determined experimentally by measuring absorption intensities of hydrous and hydroxyl bands with well established calibrations.

The absorption of a crystal can also be connected to electric properties and refractive index through the complex dielectric function (e.g., Garbuny 1965)

$$\varepsilon(\omega) = \varepsilon'(\omega) + i\varepsilon''(\omega). \quad (9)$$

The function is frequency (ω), temperature, and pressure dependent. The real and imaginary parts of the dielectric function ε are directly related to the optical constants such as the refractive index (*n*) and extinction coefficient or absorption index *k* by

$$\varepsilon' = n^2 - k^2, \quad (10)$$

$$\varepsilon'' = 2n \cdot k. \quad (11)$$

The real and imaginary parts of the complex dielectric constant are coupled through the Kramers-Kronig relation (Kramers 1926; Kronig 1926; Martin 1965)

$$\varepsilon'(\omega) = 1 + \frac{2}{\pi} P \int \frac{\omega' \varepsilon''(\omega')}{\omega'^2 - \omega^2} d\omega' \quad (12)$$

where *P* denotes the principle value of the integral. The equation essentially gives a common form of the sum rule (e.g., Brüesh 1986). Extinction coefficient *k* is connected to absorption coefficient *A*′ and light speed *c* by

$$A = 2\omega \cdot k/c. \quad (13)$$

Using Equations 11 and 13, Equation 12 can be rewritten as

$$\varepsilon'(\omega) = 1 + \frac{c}{\pi} P \int \frac{n(\omega') A(\omega')}{\omega'^2 - \omega^2} d\omega' \quad (14)$$

which gives the relationship between the absorption coefficient, the dielectric constant and the refractive index. As ε' for most materials is temperature dependent, it is obvious that the absorption coefficient in infrared spectra must also depend on temperature.

EXPERIMENTAL METHODS

SAMPLE PREPARATION AND INSTRUMENTS

Polarized infrared absorption spectra were collected from oriented crystals and thin plates (e.g., apatite and titanite). For materials with cubic crystal structures (e.g., hydrous/deuterated garnets and KNT), polarized spectroscopy does not result in spectra very different from unpolarized measurements. Infrared measurements of layered silicates were all carried out under unpolarized conditions because of their layered structures or non-perfect single crystals (e.g., sericite). Infrared spectra of the combination and overtone bands were obtained from thin sections; however, powdered samples were used for measurements of fundamental vibrations of the hydrous species in the hydrous minerals (i.e., hydrous/deuterated garnet, pyrophyllite, talc, and mica) because of their high OH concentrations and the difficulties

in obtaining plates thin enough for measuring OH fundamental bands and in handling and measuring very thin and tiny crystals with a closed-cycle liquid-helium cryostat. The KBr powder pellet technique reported by Zhang et al. (1996) was employed to dilute the sample concentrations. The IR absorption spectra recorded from thin sections were normalized by their thicknesses and given in measured absorptivity, $-\log(I/I_0)/l$, in cm^{-1} (we refer to absorptivity, rather than absorption coefficient, because of the possible weak change of species concentrations in the measured temperature range and potential surface absorption; see more details in the Discussion), whereas those obtained from powdered samples are in absorbance, $-\log(I/I_0)$. The temperature dependencies of infrared absorption bands are given by relative change of band area (the difference between integrated intensities at temperature T and 300 K vs. the integrated intensity at 300 K) so as to exclude or reduce the possible contributions of surface absorption which is expected to be less temperature dependent at low temperatures (Rowe and Harrington 1976, see later sections). The samples were gently ground with an agate mortar and pestle to avoid damage and the powdered samples were dried at 110 °C for 12 h to remove any water absorbed during grinding. Approximately 3 mg of fine sample powders were thoroughly mixed with 900 mg of dry KBr powder. About 200 mg of the sample/matrix mixtures were pressed into disk-shaped pellets with 13 mm diameter at room temperature under vacuum. The pellets were baked at 110 °C for 1–2 h to remove any surface-absorbed H_2O, and measurements were carried out within 12 h of the preparation. For single-crystal measurements, the crystallographic orientations of the crystals were determined using external morphology, X-ray precession techniques, and a polarizing light microscope. Crystal plates were cut in the required orientations and were subsequently polished.

All the IR measurements were carried out in the Bruker Vibrational Spectroscopy Lab in the Department of Earth Sciences, University of Cambridge. Using a Bruker IFS 113v spectrometer, absorption spectra between 20 and 300 K were recorded under vacuum to avoid absorption from water and carbon dioxide in the air. The spectra were measured in four separated frequency regions with different instrumental arrangements: (1) 500–4000 cm^{-1} (KBr pellets, MCT detector, Ge/KBr beamsplitters, Globar lamp, KRS5 windows for the cryostat); (2) 1250–5000 cm^{-1} (oriented thin sections of crystals, MCT detector, Ge/KBr beamsplitter, Globar lamp, KRS5 windows for the cryostat); (3) 3000–5000 cm^{-1} (thin sections of clays, MCT detector, Si/CaF_2 beamsplitter, tungsten/Globar lamp, quartz windows for the cryostat); and (4) 6000–8000 cm^{-1} (thin sections of other layer silicates, InSb or MCT detector, Si/CaF_2 beamsplitter, tungsten lamp, quartz windows for the cryostat). In each spectral range, measurements were repeated on cooling and the spectra were reproducible. Instrumental resolutions ranging from 0.1 to 4.0 cm^{-1} were tested and most data were recorded with an instrumental resolution of 0.2 cm^{-1}. Either 200 or 1000 scans were averaged.

A closed-cycle liquid-helium cryostat (LEYBOLD), equipped with KRS5 and quartz windows, was used to maintain low temperatures. Two thermal sensors were used: one to control the cryostat and the other to measure the sample temperature. Temperature stability was better than 1 K.

Influence of experimental conditions on the peak profiles of hydroxyl species

Different combinations of sources, detectors, and beamsplitters were used to test their potential influence on the peak profiles of hydrous species in two frequency ranges (3000–5000 and 6000–8000 cm^{-1}). Although different experimental arrangements show different sensitivities, the variations caused by the experimental conditions (i.e., choice of detectors, beamsplitters, and sources) on the measured data in terms of absorbance were small (<1%). To compensate for the fact that low sensitivity leads to lower signal-to-noise ratios, a longer recording time is required. We noted that between 3000 and 5000 cm^{-1}, the combination of a liquid-nitrogen-cooled MCT detector, a KBr beamsplitter, and a Globar source gives the best data reproducibility. The other commonly used combination (a liquid-nitrogen-cooled InSb detector, a CaF_2 beamsplitter, and a tungsten lamp) is best for the 6000–8000 cm^{-1} region. Although the CaF_2 beamsplitter is IR transparent down to 650 cm^{-1}, its coupling with a tungsten lamp and a liquid-nitrogen-cooled InSb detector causes spectra near 3000 cm^{-1} to become distorted, likely because of the limitation of the infrared source, the beamsplitter, and the response of the detector. The possible influence of long-term instrumental stability, especially in the NIR region, was also checked. Our results show that after a warm-up period of three hours, the time-dependence of the measured absorbance was small (<0.4%) for NIR, and could be even lower in the MIR region (coupled with Globar lamp, KBr beamsplitter, MCT detector, 250 scans, and instrumental resolution of 1 cm^{-1}). The main influence appears to be from the vacuum and the gradual heating of the Globar lamp. However, for the NIR region and the combination of a liquid-nitrogen-cooled InSb detector, a CaF_2 beamsplitter, and a tungsten lamp, a warm-up period of at least five hours is recommended if absolute values are required. We also noted that the vacuum quality has significant effects on the long-term stability of the instrument, the signal-to-noise ratio and the overall baseline. As the temperature of the lab was set to 18 °C during the experiments and the infrared spectrometer had a stabilized power supply, we consider that the possible thermal expansion of the optical bench of the infrared spectrometer and electrical fluctuations during the experiments had either no influence or an undetectable small influence on the results.

Insufficient instrumental resolution may dramatically affect the spectral features, especially the linear and integral absorbances. In this study, IR data for pyrophyllite and talc were obtained with instrumental resolutions of 0.1, 0.2, 0.3, 0.5, 1.0, 2.0, and 4.0 cm^{-1} in the frequency region of 2000 and 7500 cm^{-1}. The data show that at room temperature, the spectral features of pyrophyllite recorded at 0.1 cm^{-1} (1000 scans) and 2.0 cm^{-1} (250 scans) are essentially indistinguishable, although the spectrum recorded at 0.1 cm^{-1} has a much lower signal to noise ratio (higher spectral noise) because of its much higher resolution. At 20 K, the spectrum of pyrophyllite recorded with a resolution of 0.1 cm^{-1} showed very different spectral features from that recorded with 2.0 cm^{-1}. The former showed higher absorbance and sharper bands in the OH band region. In addition, the high-resolution measurements permitted the identification of bands with wavenumbers very close to each other (see below). The data also show that the temperature evolution of the measured linear and integral absorbance can be strongly affected by insufficient instrumental resolution, and that high resolution is required for some sharp bands.

The temperature dependencies of IR bands of OH species can also be affected by the methods used to analyze the data, especially in the NIR region, as the bands in this region are relatively broad and overlapping. Curve fitting may not be the best way to extract the integral absorption or the area of a band. When the quality of spectral data are as good as those obtained in the present study, integration using a linear baseline over a given wavenumber region gives lower data scatter and smaller standard deviations in comparison with those obtained by curve-fitting, probably because of the flat baselines of the spectra. Other factors that may affect the outcome of the analysis to a different extent are baseline shapes, the regions over which the baseline corrections were carried out, and peak-fitting functions. Investigation of the impact of these factors was beyond the scope of the present study, although previous studies have considered some of them (e.g., Behrens et al. 1996; Withers and Behrens 1999; Keppler and Rauch 2000). In our curve-fitting analysis, linear baselines between the two absorption minima and the Lorentzian function were used. The OH spectra presented here are of high quality and most have essentially flat backgrounds, so the use of linear baselines is thought not to have led to significant differences in the analysis.

RESULTS

HYDROUS MINERALS: SYNTHETIC HYDROUS/DEUTERATED GARNETS AND APATITE

Synthetic $Ca_3Al_2(O_4D_4)_3$ and $Ca_3Al_2(O_4H_4)_3$ were studied as examples of hydrous minerals. The materials, which crystallize with cubic structures, were synthesized by the method of Lager et al. (1987) and were previously studied by Lager et al. (2005). Only powder absorption spectra in the OH fundamental region were recorded because the samples are in powdered form and also because it is difficult if not impossible to carry out polarized single-crystal absorption measurements of such small crystals while using the closed-cycle liquid-helium cryostat for cooling. At room temperature, synthetic $Ca_3Al_2(O_4D_4)_3$ and $Ca_3Al_2(O_4H_4)_3$ show fundamental O-D and O-H stretching vibrations near 2696 and 3663 cm^{-1}, respectively (Figs. 1a and 1b). The spectral features of $Ca_3Al_2(O_4D_4)_3$ are similar to those reported by Lager et al. (2005). These vibrations are due to structurally incorporated protons (Rossman and Aines 1991). In hydrous/deuterated garnet, the SiO_4 tetrahedra are replaced by $(OH)_4$ or $(OD)_4$. Kolesov and Geiger (2005) presented a symmetry analysis of the IR and Raman modes in hydrogrossular. On cooling to 20 K, the IR-active O-D stretching feature of the deuterated garnet shifted to 2703 cm^{-1} (an increase of about 0.26%) (Fig. 1a), and whereas the O-H

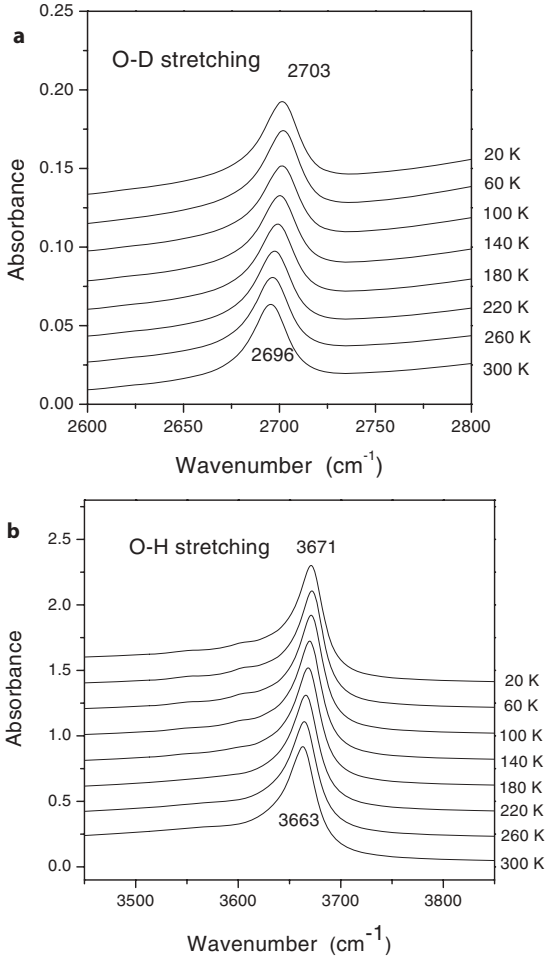

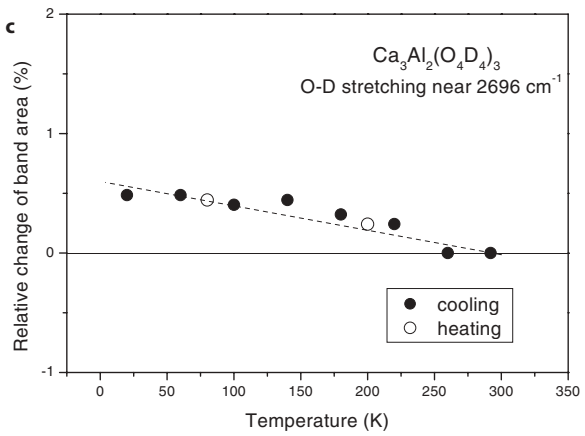

FIGURE 1. (**a**) IR powder absorption spectra of $Ca_3Al_2(O_4D_4)_3$ between 20 and 300 K (the spectra are shifted for clarity); (**b**) IR powder absorption spectra of O-H stretching bands between 20 and 300 K (the spectra are shifted for clarity); and (**c**) temperature dependence of the integrated band intensity (i.e., the band area between 2650 and 2750 cm^{-1} after linear baseline corrections) of the O-D stretching band near 2696 cm^{-1}. The lines are visual guides. The OH and OD bands of hydrous/deuterated garnets show weak changes in absorption between 20 and 300 K.

stretching feature of hydrous garnet increased to 3671 cm^{-1} (an increase of approximately 0.22%) (Fig. 1b). The formation of additional bands was not observed in the spectra of $Ca_3Al_2(O_4H_4)_3$ and $Ca_3Al_2(O_4D_4)_3$, even at 20 K. The lack of IR bands for ice at 20 K suggests that any possible H_2O absorbed in the sample pellet preparation was removed by drying the powdered sample and pellet at 110 °C (see above). To further confirm the observation in the IR measurements, Raman spectra of synthetic $Ca_3Al_2(O_4D_4)_3$ and $Ca_3Al_2(O_4H_4)_3$ were also recorded at room temperature and 80 K with a LabRam micro-Raman system (laser excitation of 632 nm, CCD detector, grating with 1800 grooves/mm, and 50× ultra-long working-distance objective) and a Linkam liquid-nitrogen cooling stage. At room temperature, the O-D stretching vibrations in $Ca_3Al_2(O_4D_4)_3$ give rise to a Raman feature near 2694 cm^{-1} with a measured full width at half height of about 20 cm^{-1}, while synthetic $Ca_3Al_2(O_4H_4)_3$ gives rise to a Raman feature near 3651 cm^{-1} with a bandwidth, full width at half height, of about 30 cm^{-1}. The relatively broad bandwidths indicate that the Raman features consist of multiple bands. At 80 K, the Raman feature of the O-D vibrations shifts to 2703 cm^{-1} (a change of 0.33%) and the O-H Raman signal moves to 3665 cm^{-1}. The frequency change seen in the Raman spectra is consistent with the results from the IR measurements. The IR intensity of these bands exhibits little or no temperature dependence on cooling.

For instance, the integral IR absorbance (between 2650 and 2750 cm^{-1} after a linear baseline correction) of the 2696 cm^{-1} band (O-D stretching) showed a 0.5% increase at 20 K (Fig. 1c), which is around the limit of the sensitivity of the measurement. In the present study, the temperature dependence of integral or linear absorbance is given in terms of the relative change (i.e., the difference between the given temperature and room temperature values divided by the room-temperature value), as it better describes the effect of temperature on the band absorption than the absolute numbers. Kolesov and Geiger (2005) also reported vibrational spectra for a single-crystal of katoite [$Ca_3Al_2(O_4H_4)_3$] at low temperatures. Although the OH spectra recorded at room temperature are very similar in both studies, the data from their single crystal showed that the main OH feature near 3660 cm^{-1} consists of several weak components below 80 K. These were not resolved in the present measurements from powdered samples even with a much higher instrumental resolution (0.2 cm^{-1}). However, it is difficult to compare the changes of OH species seen in the single crystals and the powders because of their different lattice perfections, possible water at grain boundaries, and possible fluid inclusions.

A single crystal of apatite [$Ca_5(PO_4)_3(OH,F,Cl)$] originating from Malmberget, Sweden, was also investigated. The crystal showed principal spectral features similar to those reported by Shi et al. (2003) for a natural apatite crystal, implying their close or similar chemical compositions. Polarized IR spectra (between 1650 and 5000 cm^{-1}, 20–300 K, and **E** || **c**) are shown in Figure 2a. We know from previous studies that the dipole of OH ions in apatite is parallel to the **c**-axis (see Elliott 1994 for reviews). Consistent with previous observations, our data obtained with **E** ⊥ **c** show essentially flat spectra in the OH fundamental region. Absorption features in the region 1950–2250 cm^{-1} are due to the

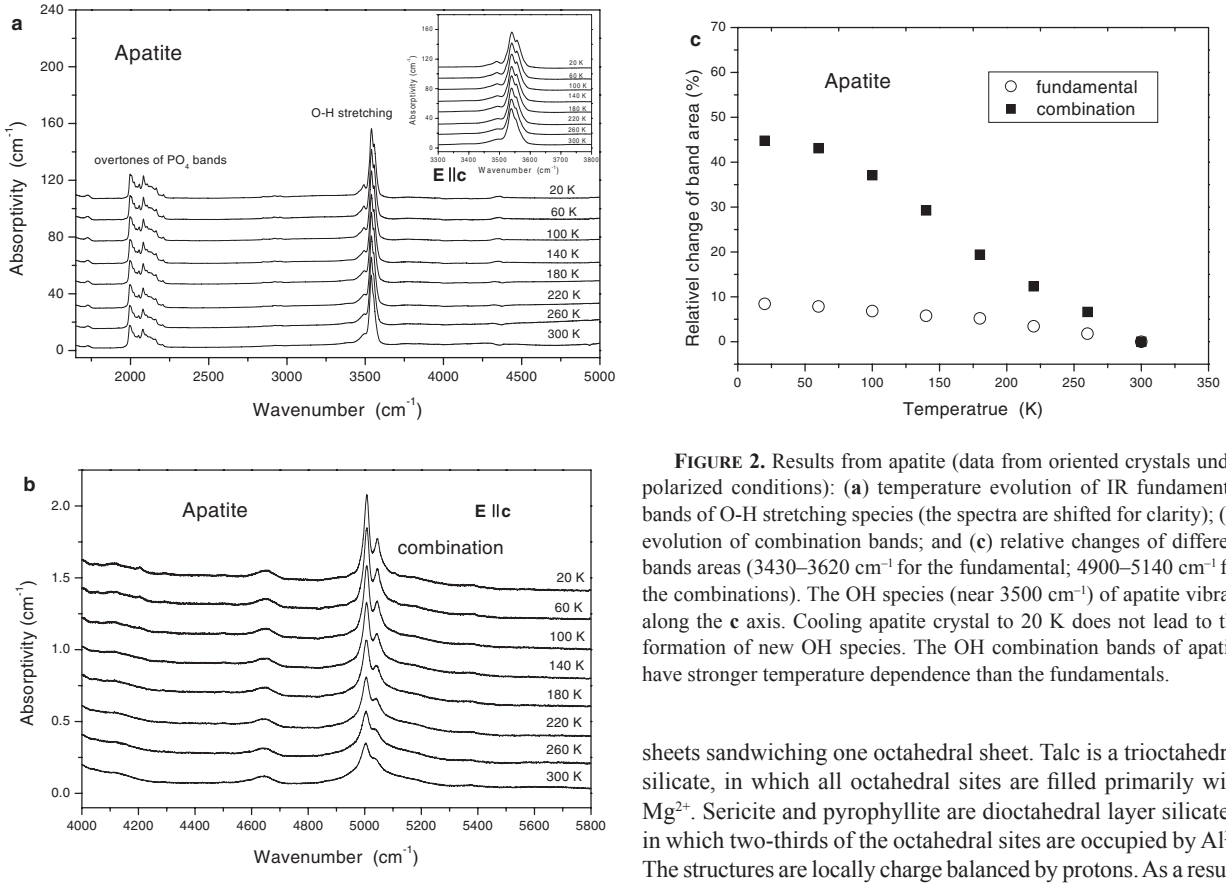

FIGURE 2. Results from apatite (data from oriented crystals under polarized conditions): (**a**) temperature evolution of IR fundamental bands of O-H stretching species (the spectra are shifted for clarity); (**b**) evolution of combination bands; and (**c**) relative changes of different bands areas (3430–3620 cm^{-1} for the fundamental; 4900–5140 cm^{-1} for the combinations). The OH species (near 3500 cm^{-1}) of apatite vibrate along the **c** axis. Cooling apatite crystal to 20 K does not lead to the formation of new OH species. The OH combination bands of apatite have stronger temperature dependence than the fundamentals.

first overtone of the stretching vibrations of the PO_4 groups (Shi et al. 2003). Absorption bands near 3493.0, 3538.1, and 3553.2 cm^{-1} (Fig. 2a) are associated with O-H stretching vibrations. The 3493.0 cm^{-1} band is due to OH groups which are hydrogen-bonded to fluoride ions and the 3538.1 cm^{-1} band is associated with OH species bonded to chloride ions (Levitt and Condrate 1970; Dahm and Risnes 1999). These bands shifted to 3491.6, 3540.1, and 3557.6 cm^{-1} at 20 K, respectively. The single-crystal spectra also reveal combination bands of hydroxyl groups near 4644.7, 5003.6, and 5038.8 cm^{-1} (Fig. 2b). On cooling, these bands shifted to 4651.6, 5007.6, and 5045.8 cm^{-1} at 20 K, respectively. The integral absorption of the fundamental OH bands and the combinations was obtained by integrating the band area in the 3430–3620 and 4900–5140 cm^{-1} regions with linear base lines (Fig. 2c). For the combination bands, the relative change of the band areas shows a much stronger temperature dependence on cooling to 20 K. An increase of about 50% was observed, which is roughly four times higher than the value (~9%) for the fundamental vibrations of the hydroxyl groups. No evidence was found in the present study for the disappearance or the formation of new species with **E** || **c** and **E** ⊥ **c** on cooling.

Layer silicates: Talc, mica (sericite), and pyrophyllite

Talc, muscovite (sericite), and pyrophyllite were chosen for the present study because they are typical layer silicates with similar crystal structures (Deer et al. 1992). They all have 2:1 layered structures, i.e., the layers consist of two tetrahedral silicate sheets sandwiching one octahedral sheet. Talc is a trioctahedral silicate, in which all octahedral sites are filled primarily with Mg^{2+}. Sericite and pyrophyllite are dioctahedral layer silicates, in which two-thirds of the octahedral sites are occupied by Al^{3+}. The structures are locally charge balanced by protons. As a result, they contain structural hydroxyl contents amounting to 4–5 wt% H_2O. More detailed information on these minerals can be found in the reviews by Bailey (1988) and Mottana et al. (2002).

A talc sample (LHC01) originating from Haicheng, Liaoning Province, China, was investigated. Electron microprobe analysis showed that the bulk sample has a composition that is close to the ideal $Mg_3(Si_4O_{10})(OH)_2$ (Zhang et al. 2006). At room temperature, sample LHC01 shows a sharp absorption band with a full width at half maximum of about 5 cm^{-1} near 3676 cm^{-1} (Fig. 3a). In talc, the hydroxyl ion is believed to be symmetrically linked to three Mg ions, and the 3676 cm^{-1} band has been assigned to O-H stretching due to the Mg_3OH species (Wilkins and Ito 1967; Russell et al. 1970; Petit et al. 2004; Zhang et al. 2006). Sample LHC01 exhibits several features with peaks at 4055, 4182, 4332, and 4369 cm^{-1} (Figs. 3b and 3c) which are associated with combinations. The first overtone bands of the O-H stretching appear near 7185 cm^{-1} (Petit et al. 2004; Zhang et al. 2005).

The temperature evolution of IR spectra of talc measured in three wavenumber regions is presented in Figures 3a–3c. The spectra show a dramatic change in the first overtone features, although the spectrum of the fundamental bands recorded at 20 K is not significantly different from that measured at 300 K. Cooling to low temperatures reveals that the overtone feature consists of three individual bands (observed using an IR instrumental resolution of 0.2 cm^{-1}). At 20 K they are located at 7180.6, 7184.2, and 7187.6 cm^{-1}, all with a bandwidth of ~1.6–2.1 cm^{-1}. The bands at 7180.6 and 7184.2 cm^{-1} have not been observed prior to the present study. At room temperature,

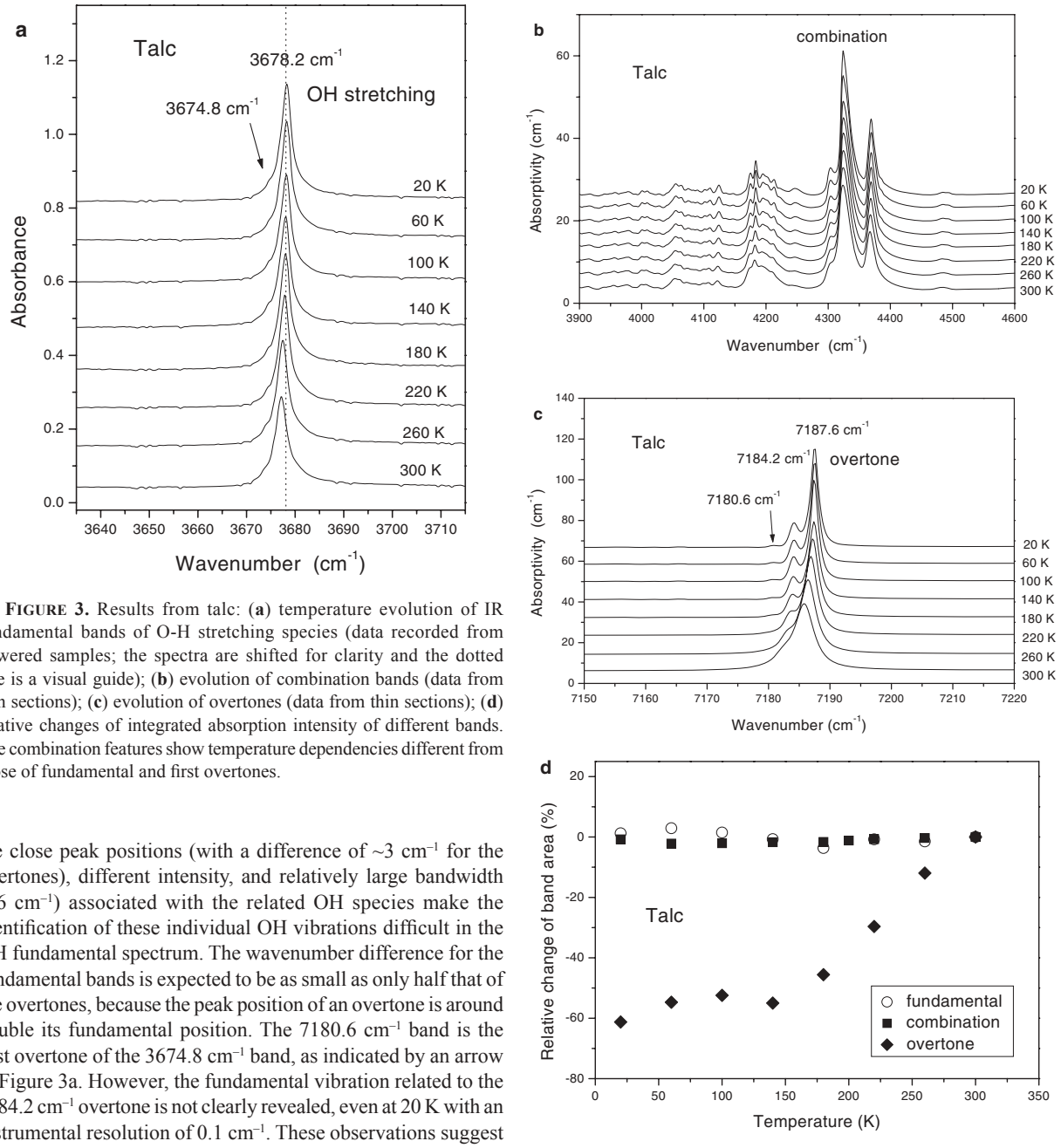

FIGURE 3. Results from talc: (**a**) temperature evolution of IR fundamental bands of O-H stretching species (data recorded from powered samples; the spectra are shifted for clarity and the dotted line is a visual guide); (**b**) evolution of combination bands (data from thin sections); (**c**) evolution of overtones (data from thin sections); (**d**) relative changes of integrated absorption intensity of different bands. The combination features show temperature dependencies different from those of fundamental and first overtones.

the close peak positions (with a difference of ~3 cm^{-1} for the overtones), different intensity, and relatively large bandwidth (~6 cm^{-1}) associated with the related OH species make the identification of these individual OH vibrations difficult in the OH fundamental spectrum. The wavenumber difference for the fundamental bands is expected to be as small as only half that of the overtones, because the peak position of an overtone is around double its fundamental position. The 7180.6 cm^{-1} band is the first overtone of the 3674.8 cm^{-1} band, as indicated by an arrow in Figure 3a. However, the fundamental vibration related to the 7184.2 cm^{-1} overtone is not clearly revealed, even at 20 K with an instrumental resolution of 0.1 cm^{-1}. These observations suggest that low-temperature data from the overtone region are useful for identifying overlapping fundamental bands. Integral absorbances of the OH fundamental, combination, and overtone bands have been obtained by integrating the related wavenumber regions of the IR spectra with separate linear baselines. Their relative changes are plotted as a function of temperature in Figure 3d. It is interesting to note that the integrals of the fundamental and combination bands exhibited almost no temperature dependence, whereas the overtone showed a significant decrease in integral absorption with falling temperature.

Sericite is a fine-grained variety of muscovite, a dioctahedral silicate with the ideal chemical formula $(K,Na)Al_2[AlSi_3O_{10}](OH)_2$. The $2M_1$ polytype of muscovite has a monoclinic structure (*C*2/c) (Mottana et al. 2002). Tetrahedral sheets are linked together by alternating layers of K^+ and octahedral Al^{3+}. The $2M_1$ sample investigated in the present study is from the sericite deposit in Song County, Henan Province, China, and more information about it can be found in Pei and Shi (1996) and Zhang et al. (2005).

The powder IR absorption spectrum from this sample shows three bands near 3629.8, 3645.4, and 3660.4 cm^{-1} [revealed through calculating the second-order derivative of the spectrum with the algorithm of Savitzky and Golay (1964)] (Fig. 4a), which are due to the O-H stretching vibration of the structurally incorporated hydroxyl groups (Aines and Rossman 1985; Zhang

et al. 2005). Combinations of the O-H stretching bands with other OH^- vibrations (e.g., the OH^- libration near 920 cm^{-1}) appear at 4106.7, 4261.3, and 4544.8 cm^{-1}, and the first overtone bands related to the O-H stretching bands near 3630 cm^{-1} are found in the region between 7050 and 7200 cm^{-1} (Figs. 4b and 4c). Cooling sericite to low temperatures led to weak changes in the OH spectra, in contrast with the thermal behavior of talc as described above. The 3629.8, 3645.4, and 3660.4 cm^{-1} bands recorded at room temperature shifted to 3634.4, 3650.2, and 3665.0 at 20 K, respectively. A weak band near 3625.2 cm^{-1} was also resolved at 20 K. Cooling did not cause changes as significant as those observed from talc in the peak positions of the combination and overtone bands. The combination band near 4544.8 cm^{-1} shifted to 4546.4 cm^{-1} (Fig. 4b), and the band near 7084.6 cm^{-1} (first overtone) shifted to 7090.6 cm^{-1} (Fig. 4c). It is interesting to note that these features did not become significantly sharpened, even at 20 K. Integral absorption for the different types of absorption bands is shown as a function of temperature in Figure 4d. The OH overtone bands in sericite exhibit the strongest temperature response (about a 10% increase on cooling from 300 to 20 K), whereas the band areas for the fundamentals increase by 4% and the value for the combination bands is scattered around zero.

Pyrophyllite, $Al_2Si_4O_{10}(OH)_2$, is a 2:1 aluminosilicate in which two-thirds of the available octahedral sites are occupied by Al and the remainder are empty (Bailey 1966; Rayner and Brown 1966; Wardle and Brindley 1972). Two pyrophyllite samples (EM08 and SK06) were investigated. Sample EM08 is a pyrophyllite (2*M* + 1*Tc*) from the Emei pyrophyllite deposit, Fuzhou, China. Sample SK06 is a pyrophyllite (2*M*) from the Shankou pyrophyllite deposit, Qingtian, China. The chemical compositions of the both samples are almost identical to the ideal composition of pyrophyllite. The samples were used in a previous study of the dehydration mechanism of pyrophyllite (Wang et al. 2002, 2003).

Infrared spectra of pyrophyllite recorded for three infrared regions and in the temperature region between 20 and 300 K are shown in Figures 5a–5c. Hydroxyl species in pyrophyllite show a strong absorption band near 3675.4 cm^{-1} (with a width of ~6 cm^{-1}) at room temperature (Fig. 5a). This feature is due to OH stretching vibrations (fundamentals). Pyrophyllite shows complex combination bands between 3800 and 5000 cm^{-1} (Fig. 5b) and first overtone bands near 7176.0 cm^{-1} (Fig. 5c). The effect of cooling is indicated by a systematic change of the peak profile of the fundamental bands of hydroxyl groups (increase in absorption, frequency shift, and line sharpening, Fig. 5a). Cooling causes different changes to the multi-phonon OH bands. The first OH overtone near 7176.0 cm^{-1} shows considerable sharpening and increase in absorbance, whereas the combination bands near 4550 cm^{-1} give rise to much weaker temperature dependencies. These two features show different temperature dependencies

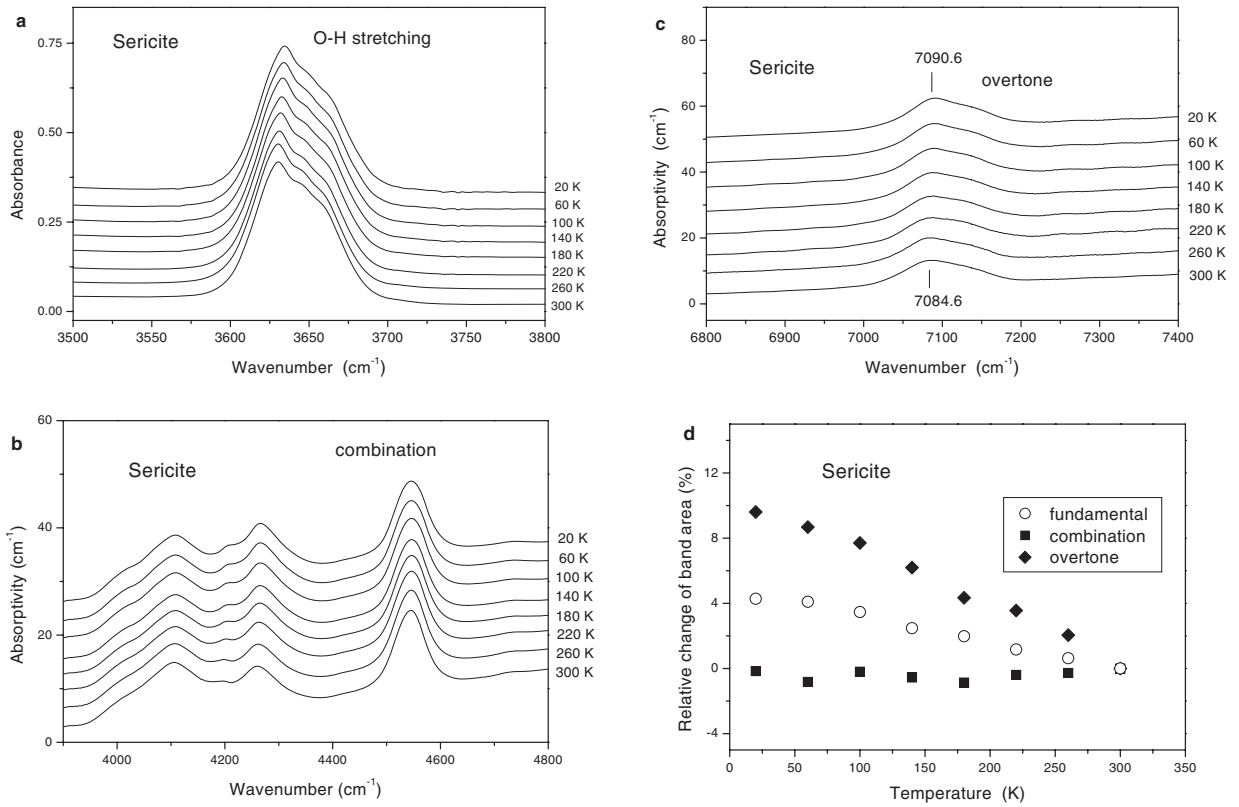

FIGURE 4. Results from sericite: (**a**) temperature evolution of IR fundamental bands of O-H stretching species (data from powered samples); (**b**) evolution of combination bands (data from thin sections); (**c**) evolution of overtones (data from thin sections); and (**d**) relative changes of different bands. The first overtone bands of the OH species show strong temperature dependence (about 10% change in band area between 20 and 300 K), whereas the combination bands are almost independent of temperature.

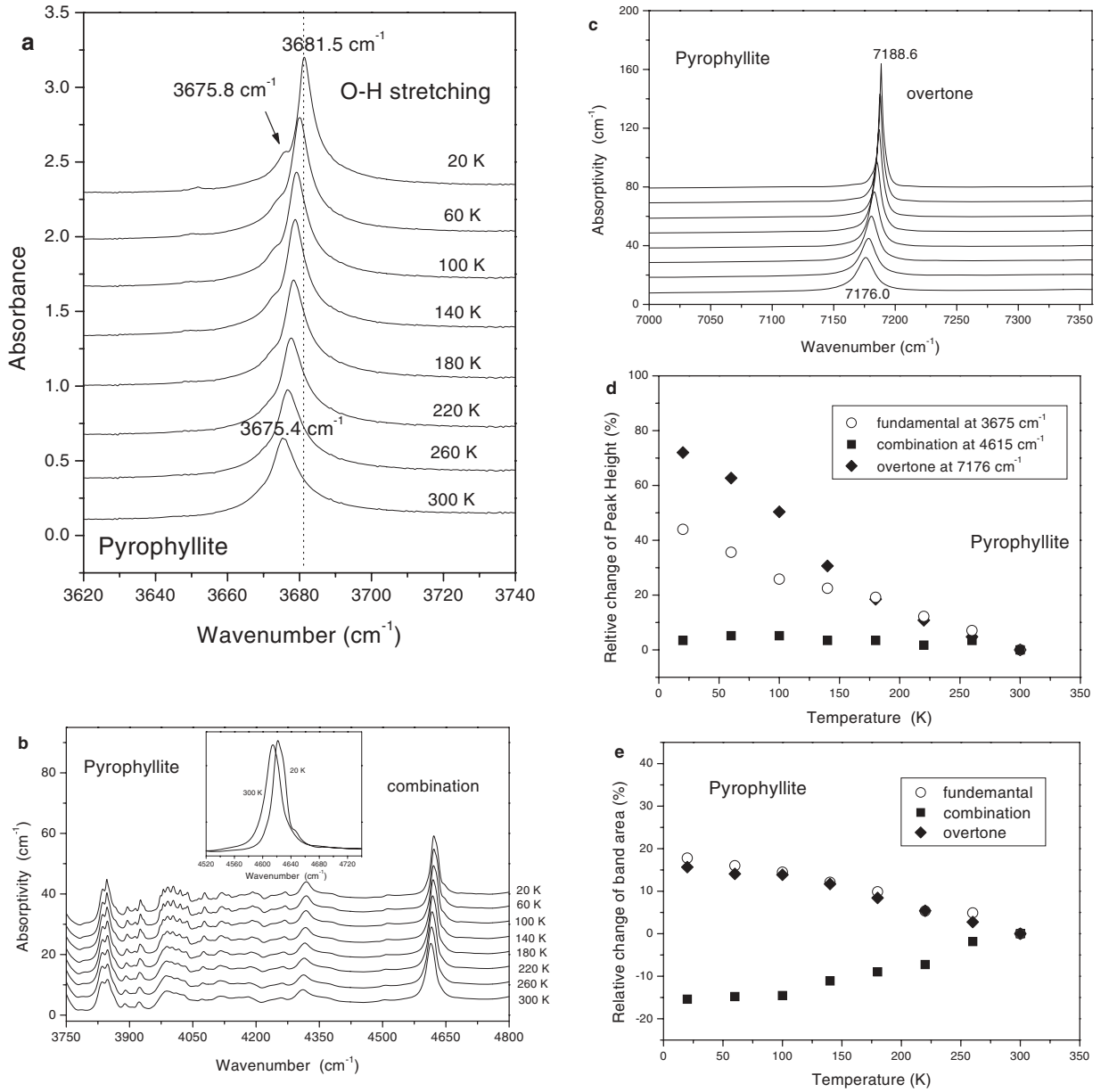

FIGURE 5. Results from pyrophyllite: (**a**) temperature evolution of IR fundamental bands of O-H stretching species (data from powdered samples); (**b**) evolution of combination bands (data from thin sections); (**c**) evolution of overtones (data from thin sections); (**d**) relative changes of absorption intensity (band heights); and (**e**) relative changes of integrated intensity (band areas). Peak heights and band areas of pyrophyllite display different temperature evolution. The overtone band near 7176 cm^{-1} shows a 72% relative change in band absorption height between 20 and 300 K, in contrast to only 16% change in integrated band area.

for their linear absorption (i.e., the band height) (Fig. 5d) and their integrated absorption intensity (band area) (Fig. 5e). The data in Figures 5d and 5e also indicate that the linear absorption and integrated absorption do not show the same changes. As there is no evidence for the formation of additional OH bands on cooling, it appears that the changes in IR absorption shown by the OH species are simply due to cooling-related structural compression and a consequent change of the dipole moments of the ions.

A nominally anhydrous mineral: titanite

Pure titanite ($CaTiSiO_5$) is monoclinic, space group $P2_1/a$ ($Z = 4$), with unit-cell parameters $a = 7.057$, $b = 8.707$, $c = 6.555$ Å, and $\beta = 113.81°$ (Taylor and Brown 1976). The crystal structure consists of chains of corner-sharing TiO_6 octahedra along [100] that are cross-linked by chains of edge-sharing CaO_7-polyhedra parallel to [101]. SiO_4 tetrahedra are linked by corners to both structural units (Taylor and Brown 1976; Speer and Gibbs 1976).

The 20 O atoms per unit cell are located at three different sites. Among these, only O(1) is not connected to SiO_4 tetrahedra and can be occupied by OH or F. The direction of the O-H dipoles is oriented in the (010) plane. The OH species lead to a sharp infrared absorption near 3486 cm^{-1} in spectra for crystalline titanite, which exhibits an absorption maximum when **E** is approximately parallel to the direction of the refraction index n_α (Isetti and Penco 1968; Beran 1970). Three titanite crystals (samples No12, B20323, and Rauris) were analyzed in the present study because additional OH bands occurred at low temperatures. These crystals have been characterized previously (Hammer et al. 1996; Meyer et al. 1996; Zhang et al. 1997, 2001) and more information is listed in Table 1. Measurements of sample No12 were obtained from the (010) surface, whereas the data for the Rauris sample were recorded from an unoriented crystal. Spectra of sample B20323 were obtained from a surface nearly parallel to (101) (with an off-plane angle of 3°). The nuclear-reaction analysis carried out by Hammer et al. (1996) showed that the average hydrogen concentration in sample No12 corresponds to about 0.15 wt% H_2O. Detailed information about the samples from the previous studies is given in Table 1.

The incorporated hydroxyl species give rise to an IR feature near 3486 cm^{-1} (Figs. 6a and 6b). Cooling leads to a significant increase in the OH band absorbance (band height) and band sharpening (Figs. 6a–6c). The main OH feature near 3486 cm^{-1} in Figure 6a shows a strong relative increase in linear absorbance (82% with **E** || n_α and 81% with **E** || n_γ) from 300 to 20 K. This result is consistent with the data from unpolarized measurements of sample B20323 (Fig. 6b), which exhibits an increase of 79%. The observations indicate that titanite absorption measured under both polarized and unpolarized conditions shows essentially the same relative change or temperature gradient. In contrast to the significant variation of linear absorbance between 20 and 300 K, the integral absorbance (between 3350 and 3650 cm^{-1}) of this OH fundamental feature has much weaker temperature dependence (4.5% with **E** || n_α for sample No12 and 4.2% from unpolarized measurements of B20323). Similar to some minerals described in earlier sections, the OH combination bands of titanite have different temperature dependencies than the fundamental bands. For example, the combination band near 4545 cm^{-1}, which has a high intensity with **E** || n_γ and shifts to 4556 cm^{-1} at 20 K (Fig. 6a), shows relative changes of 121.0% in linear absorbance (i.e., band height) and 66.6% in integral absorbance between 4510 and 4600 cm^{-1} (with **E** || n_γ) on cooling from 300 to 20 K. We did not attempt to extract the values of the combination band for the case of **E** || n_α due to its low intensity, which might affect the outcome, especially the baseline-sensitive integrated intensity. Two unexpected changes were observed in the cooled titanite samples. First, the feature near 4418.2 cm^{-1} in sample B203023 showed interesting spectral tends at temperatures below 240 K. These include a shift to 4418.6 cm^{-1} at 240 K, a shape change near 200 K, and band splitting (to 4403.0 and 4426.4 cm^{-1}) at 220 K, with these bands exhibiting shifts as temperature decreases to 20 K (Figs. 6b and 6d). The band-splitting-like behavior of the 4418.2 cm^{-1} band in titanite (Figs. 6b and 6d) is unusual. It appears to indicate a modification of local symmetry, but this hypothesis is not fully consistent with previous studies in which structural changes in the titanite crystals at low temperatures were not observed (e.g., Zhang, M. et al. 2000). This observation could be due to the fact that OH ions are very sensitive to their local environments; they can "see" or respond to very weak changes, which are too subtle for other methods to detect directly. Second, the Rauris sample showed a dramatic change of spectral pattern on cooling because of the development of two bands near 3120 and 3216 cm^{-1}. However, the band near 3565 cm^{-1} became almost undetectable on cooling (Fig. 6c; the upward and downward pointing arrows indicate that the band intensity increased or decreased on cooling). A similar change was also observed in samples B20323 and No12, although from the recorded spectra the change appeared weak in these crystals, probably because of their different crystallographic orientations. The development of additional bands and the disappearance of the 3565 cm^{-1} band on cooling imply the formation of strongly hydrogen-bonded OH defects, replacing oxygen positions that belong to the isolated SiO_4 units. The presence of the band at 3565 cm^{-1} at room temperature and its decease in intensity at lower temperatures could be explained by hydrogen diffusion, resulting in the formation of OH groups with a slightly different local environment in comparison with OH groups related to the 3486 cm^{-1} band.

An anhydrous material: Synthetic cubic KTN ($KTa_{1-x}Nb_xO_3$)

Cubic KTN ($KTa_{1-x}Nb_xO_3$) is one of the most promising photorefractive materials that has applications in electro-optic devices such as wavelength filters and switches (Agranat et al. 1989). The $KTa_{1-x}Nb_xO_3$ (KTN, x = 0.37) samples used in the present study were single crystals. They were synthesized by the top-seeded flux method (Wang et al. 1992a). Detectable amounts of hydrogen are incorporated into the material during crystal growth. On cooling, KTN undergoes a series of phase

TABLE 1. Details of samples

Samples	Description	Symmetry	Localities/synthesis	References
CAOD	$Ca_2Al_2(O_4D_4)_3$	cubic	synthetic	1
CAOH	$Ca_2Al_2(O_4H_4)_3$	cubic	synthetic	1
19796-4	apatite	hexagonal	Malmberget, Sweden	
LHC01	talc	monoclinic	Haicheng, Liaoning, China	2
HZ08	mica (sericite)	monoclinic	Haungzhuang, Henan, China	3, 4
EM08	pyrophyllite	monoclinic	Emei, Fuzhou, China	5
SK06	pyrophyllite	monoclinic	Shankou, Qingtian, China	5
No12	titanite	monoclinic	Austria	6, 7
B20323	titanite	monoclinic	unknown	7–9
Rauris	titanite	monoclinic	Austria	7–9
KTN	KTN	cubic	synthetic	10

Note: 1 = Lager et al. (1987, 2005); 2 = Zhang et al. (2006); 3 = Pei and Shi (1996); 4 = Zhang et al. (2005); 5 = Wang et al. (2002, 2003); 6 = Hammer et al. (1996); 7 = Zhang et al. (2001); 8 = Meyer et al. (1996); 9 = Zhang, M. et al. (1997, 2000); 10 = Wang et al. (1992a, 1992b).

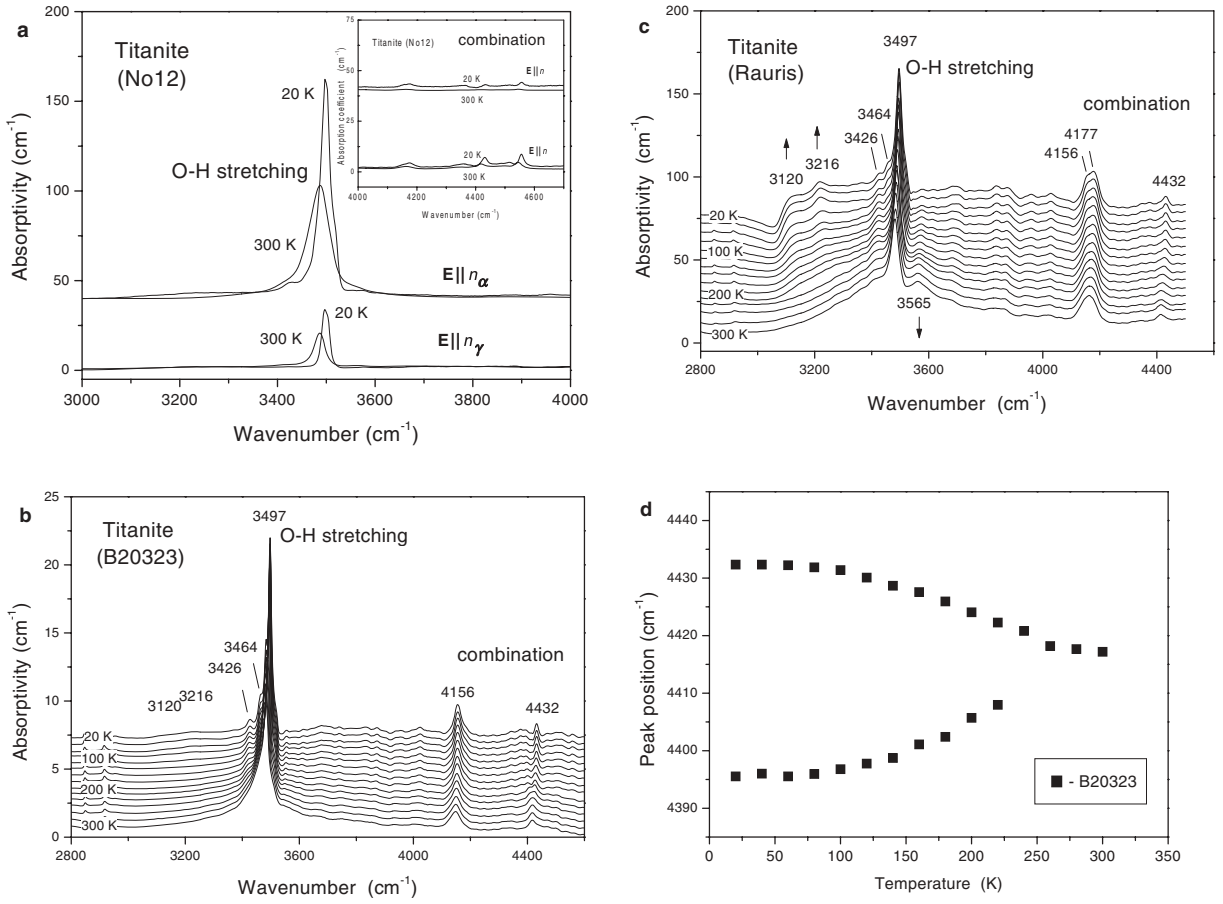

FIGURE 6. Results from crystalline titanite samples: (**a**) termperature evolution of the IR bands of sample No12 [polarized data recorded from the (010) plane]; (**b**) B20323 [unpolarized data from a plane nearly parallel to (101)]; (**c**) sample Rauris (data from unoriented crystal); and (**d**) peak positions of IR combination bands of sample B20323.

transitions (cubic-tetragonal-orthorhombic) (e.g., Wang et al. 1992b). Infrared measurements were carried out on crystal slices cut parallel to (100). Although the presence of protons and hydroxyl groups in KTN has been reported (e.g., Imai et al. 1996), their temperature behavior has not been investigated in detail. On the other hand, the behavior of protons and OH in $KTaO_3$ and $SrTiO_3$, together with changes at low temperatures, has been the subject of several investigations (Engstrom et al. 1980; Weber et al. 1986; Sata et al. 1996). Some of these studies favored the idea that hydrogen is located close to an oxygen lattice site with the O-H dipole vibrating in the direction of the next nearest oxygen ion.

Spectra from the cubic KTN crystal showed two OH-stretching bands near 3491.6 and 3498.8 cm^{-1} at room temperature. These bands are likely to have origins similar to those observed in $KTaO_3$ (near 3485.0 cm^{-1}, Engstrom et al. 1980) and $SrTiO_3$ (3495.4 cm^{-1}, Weber et al. 1986). The OH concentration in the sample appears lower than reported for $KTaO_3$ by Engstrom et al. (1980), as the OH bands in KTN show weak absorption. In contrast to $KTaO_3$ and $SrTiO_3$ (with OH bandwidths of 1.5–2.6 cm^{-1}), the KTN sample gave much broader bands (about 9 cm^{-1}) at room temperature. On cooling, it showed a dramatic change in its spectral pattern, absorption intensity, and band frequencies (Figs. 7a–7c). An additional feature was recorded near 3490.3 cm^{-1} at 170 K. This feature consists of more than one band, as it is broad (~8 cm^{-1}) even at 20 K. The second derivative method revealed a weak shoulder near 3496 cm^{-1}. A weak absorption band was also recorded near 3467 cm^{-1} at 20 K. It is difficult to determine the temperature at which this band first appeared because of its low intensity, although it seemed to form near 170 K. It is interesting to note that the additional feature near 3490 cm^{-1} showed a decrease in frequency on cooling, in contrast to the increase in frequencies for the other OH bands.

The occurrence of additional O-H stretching bands in KTN on cooling indicates a change of local environments caused by the structural phase transitions. The appearance of more bands in spectra from the low-temperature phases is associated with the lower symmetry of sites in the host. The sudden change of the band areas near the transition temperatures agrees with the behavior expected for the first-order phase transition shown by previous studies (e.g., Wang et al. 1992b).

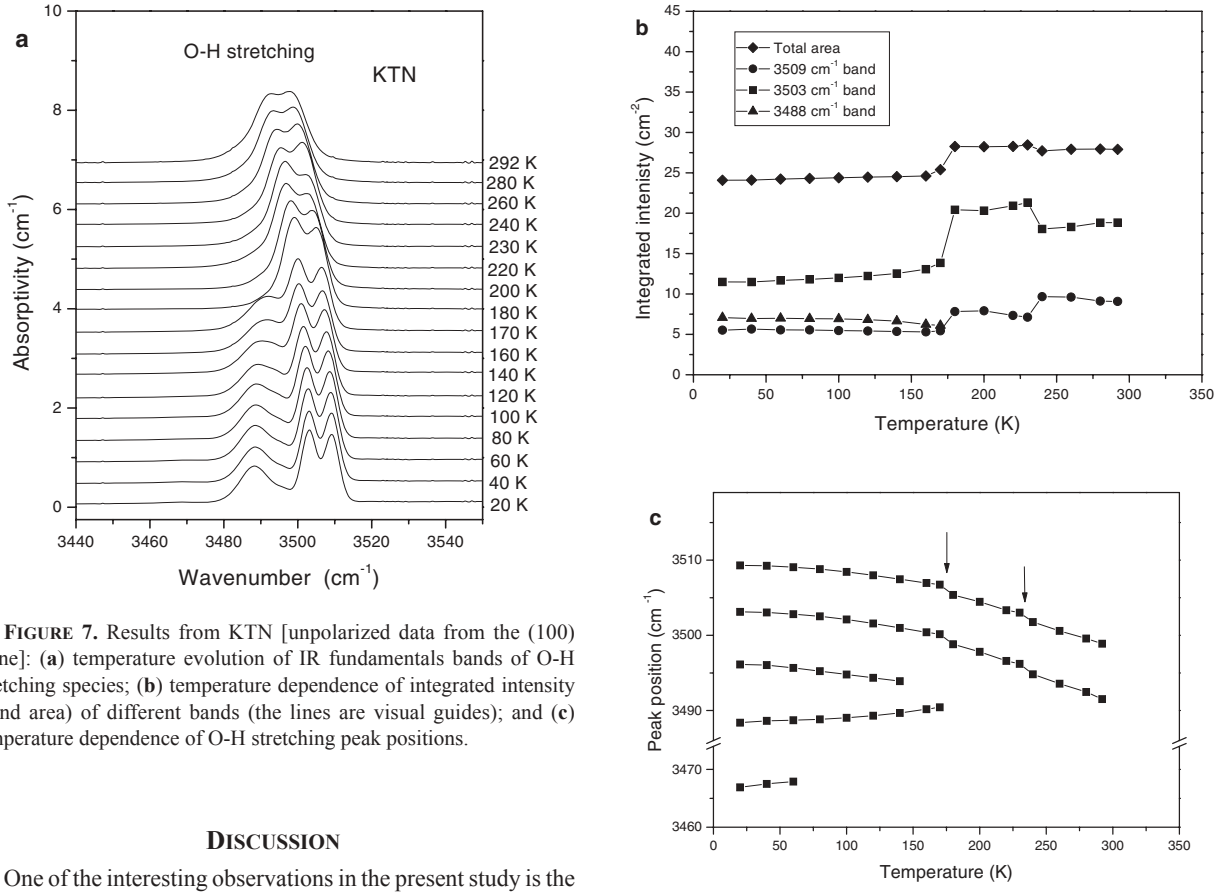

FIGURE 7. Results from KTN [unpolarized data from the (100) plane]: (**a**) temperature evolution of IR fundamentals bands of O-H stretching species; (**b**) temperature dependence of integrated intensity (band area) of different bands (the lines are visual guides); and (**c**) temperature dependence of O-H stretching peak positions.

DISCUSSION

One of the interesting observations in the present study is the different temperature dependence of OH bands in IR data from talc, muscovite (sericite), and pyrophyllite. Although all layered silicates have similar structures, cooling to low temperatures clearly had a much weaker effect on the IR bandwidths of sericite than on those of talc and pyrophyllite. The OH fundamental bands of sericite remain broad at 20 K. The combination and overtone bands recorded at 20 K also exhibit features similar to those measured at 300 K, in contrast to talc and phyrophyllite. Similar to the weak change in the bandwidths, the linear absorption coefficients or band heights of OH species in sericite do not vary much during cooling from 300 to 20 K. However, the OH band frequencies in sericite (3629.8, 3645.4, and 3660.4 cm^{-1}, at room temperature) shifted to 3634.4, 3650.2, and 3665.0 at 20 K. For talc, the OH band frequency changes from 3676.4 cm^{-1} at 300 K to 3678.2 cm^{-1} at 20 K, and for pyrophyllite the change is from 3675.4 cm^{-1} at 300 K to 3681.5 cm^{-1} at 20 K.

The causes of the difference in the thermal behavior of sericite relative to the other two layer silicates are unclear. The distinction is probably related to their different crystal structures. In contrast to the other two minerals, sericite (or muscovite) has an interlayer cation (K^+). The proton is located near the interlayer cation and one bonded oxygen along ($K\text{-}O_2$) of the basal oxygen-atom plane (e.g., Rothbauer 1971; Guggenheim et al. 1987). During cooling, the changes relating to K atoms in the layers must surely affect the behavior of the OH species. In addition, the ordering/disordering of Al/Si (Mottana et al. 2002) and deviations from the ideal orientation of the OH dipoles could influence the bandwidth of the OH bands in sericite. Perhaps the different thermal behavior of the three minerals is also connected to their dehydroxylation processes, as these differences should be associated with the local configurations of the species and structural responses to cooling-induced compression. It is interesting to note that sericite has the lowest dehydroxylation temperature (Zhang et al. 2005), in comparison with talc (Ward 1975) and pyrophyllite (Wang et al. 2002). As crystallinity and grain sizes might possibly affect dielectric constants, it is desirable to look into their possible influences on the temperature dependencies of phonon modes.

The key issue related to the results from the present study is the origin of this dramatic variations of the measured absorption intensity and the implications of the observations. If the Beer-Lambert law given by Equation 8 is considered to be valid, the observed change of absorption at low temperatures is expected to originate mainly from the changes of the absorption coefficients (although it is commonly treated as a constant in infrared analysis), the concentrations of species of interest, and the crystal thickness. The variation of crystal thickness caused by thermal expansion or contraction is not expected to make significant contributions to the observed dramatic changes of absorption intensity because values of thermal expansion coefficients for silicates and other minerals are commonly on the order of 10^{-5}/K (Knittle et al. 1986; Fei 1995), e.g., about $2.07 \cdot 10^{-5}$/K for titanite (Kunz et al. 2000) and around $0.9–1.38 \cdot 10^{-5}$/K for

muscovite (Guggenheim et al. 1987). Over a temperature range of 300 K the change of crystal thicknesses caused by thermal expansion is thus very small (e.g., estimated values are about 0.6% for titanite). For the present study, the real impact of changes in species concentration on the observed absorption should also be small or ignorable for the following reasons: (1) proton diffusion, mobility, and thermally induced reactions are not expected to be considerable because the experiments were carried out at low temperatures; (2) no intense additional IR bands of newly formed OH species were observed, and the OH bands do not show any time dependence that could occur during the diffusion- and reaction-related changes of concentrations of OH species; and (3) the relative changes of multiphonon intensity between 20 and 300 K showed variations as high as tens of percent in some cases, despite the fact that the measurements were carried out in vacuum and there were no external proton and hydrogen resources as suppliers. Assuming that the possible effect of surface absorption is irrelevant, we interpret the temperature dependence of observed absorption intensity mainly as a result of changes of absorption coefficients, whose values are sensitive to crystal structure, crystal state, and the change in dipole moments. The effects of temperature on dipole moments are complex, and are associated with the behavior of coupling constants and anharmonicity in the material studied (Cowley 1963). The mean distances between atoms in a crystal normally increase with increasing temperature. This can lead to changes of intermolecular distances and dipole moments. The other influence on the absorption is the temperature-induced variation of the coupling constants or oscillator strength (Namjoshi and Mitra 1974). The effect of temperature on the strength can be seen by the change of mode frequencies on heating or cooling, and it has a positive contribution to the temperature dependence of the absorption coefficient. Generally, crystal mode frequencies change with temperature. One phonon density state function may also shift to different frequency ranges with temperature, and the change is expected to further affect dipole moments and absorption intensity or coefficient. From the relation between dielectric constant (it is temperature dependent) and absorption coefficient given by Equation 14, it is also apparent that absorption intensity of vibration bands may change with temperature.

The strong temperature dependencies in OH multiphonon bands are particularly important. The changes are mainly due to the differences between single-phonon and multiphonon processes (Sherwood 1972; Harrington and Hass 1973; Rosenstock 1973; Schall et al. 2001). For single-phonon processes or fundamental absorptions, thermal expansion and temperature-induced changes in the nuclear coordinates or crystal energy potential are expected to result in change of dipole moments (Cowley 1963). However, for multiphonon bands, it has been generally accepted that the dependence is largely affected by temperature factors related to the overall transition probabilities of the creation and annihilation of the phonons and photon(s) involved, as well as the types (summation or difference) of phonon-phonon interactions (e.g., Fray et al. 1960; Sherwood 1972; Hardy and Agrawal 1973). The detailed temperature dependencies of absorption related to multiphonon processes are known only for some materials with simple crystal structures, such as alkali halides (e.g., Hardy and Agrawal 1973; Deutsch 1974; McNelly and Pohl 1974; Lipson et al. 1976; Bendow et al. 1978), several semiconducting materials (Bendow et al. 1977; Miles 1977), and ZrO_2 (Bendow et al. 1981), and experiments indicating temperature independences raised concerns (Sparks 1973). Early approaches (Sparks and Sham 1972; Hardy and Agrawal 1973) are mainly based on a Bose-Einstein treatment, where the temperature dependence for *m*-phonon absorption (annihilation of one photon and creation of *m* phonons) in alkali halides is proportional to

$$(\bar{n}+1)^m - (\bar{n})^m \tag{15}$$

where $\bar{n}$ is the Bose-Einstein occupation number for a phonon of frequency ω given by

$$\bar{n} = \frac{1}{e^{-\hbar\omega/kT} - 1} \tag{16}$$

where $\hbar$ and k are Planck and Boltzman constants, respectively, and T is temperature. At high temperatures, the temperature dependence can be reduced to T^{m-1} for an *m*-phonon process. These approaches predict strong temperature dependencies for high-order multiphonon overtone absorptions. Strong deviations (much weaker dependence) from the T^{m-1} dependence were observed experimentally (Harrington and Hass 1973). Improvements for the agreement between experimental data and theoretical predictions were obtained by considering thermal expansion and the temperature dependence of the phonon frequencies, the lattice constant and anharmonicity (Sparks and Sham 1973a; Maradudin and Mills 1973; Namjoshi and Mitra 1974; Rosenstock 1974; Boyer et al. 1975), and by considering phonon-phonon coupling (Rosenstock 1973).

It is worth noting that the observation of temperature dependence of multiphonon absorption can be a useful tool for separating intrinsic absorption of lattice vibrations from a perfect crystal from extrinsic absorption (associated with chemical impurities and mechanical imperfections) and for identifying the nature of bands located in multiphonon regions. These different types of multiphonon bands are believed to have very different thermal behaviors (Fray et al. 1960; Sherwood 1972; Hardy and Agrawal 1973; Sparks 1973; Rowe and Harrington 1976; Li 1980; Piccirillo et al. 2002).

The dramatic changes of absorption intensities related to OH species, especially for OH overtone bands, indicate that the Beer-Lambert law in its most simple application is not valid. Usually it is assumed that the Beer-Lambert law defines a linear relationship between the spectrum and the concentration or composition of a species or a sample, which is independent of temperature. In practice, most spectra are analyzed using a calibration parameter *a* obtained at a given temperature (e.g., most case at room temperature).The ultimate goal of the calibration is to create a calibration equation (or series of equations) or to establish a calibration model which, when applied to data of "unknown" samples measured in the same manner, will accurately predict the quantities of the species of interest. Here we have shown that such calibration has to consider the temperature dependence of the absorption coefficient when the law is applied at different temperatures and especially for multiphonon bands.

It is worth noting that the measured values of absorption

are also sensitive to crystallinity, defects, thermal history, and smoothness of the crystal surface. For anisotropic crystals, the value can also be related to polarization of the measurement or orientation conditions of the samples, although IR band intensity is mainly associated with the change of dipole moments. On heating or cooling, the variation of the OH dipole can be due to either amplitude or direction or both. The changes could potentially cause variations in relative changes (given in % in the present study) and temperature gradients (which approximates the degree of the effect of temperature on the band absorption) of integral and linear absorbance in the unpolarized spectra of anisotropic crystals. We believe that in most of the samples studied in the present investigation, the potential influence of dipole orientation on the temperature gradients and relative changes of the absorbance is not significant and its potential effect should not alter the conclusions of the present study. This is because polarized measurements of the strong OH bands from apatite and titanite (this study) and from quenched titanite (Zhang et al. 2001) do not indicate a large change of orientation of these OH vibrations (the appearance of weak bands near 3120 and 3216 cm^{-1} in titanite at low temperature is unlikely to be due to a change of orientations), and the factor is not expected to cause a real problem in results from samples with cubic structures. In fact, a change of the dipole orientation by a couple of degrees (these correspond to large changes for bond angles in common crystal structures) will be unlikely to cause a dramatic modification of absorption because its contribution to measured absorbance follows a squared cosine function. Furthermore, OH species in crystalline minerals are commonly incorporated into the crystal structures and the dipoles cannot rotate as freely as they can in liquids or even gases. Very large changes in vibration orientations of these species in the studied minerals are unlikely to take place unless there is a dramatic change of bond strength or distance, or a breaking of bonds and a modification of local symmetry, which can result in dramatic variations in OH spectra, formations of new OH species, and large changes in the frequencies of the OH bands. However, these changes do not occur in the samples investigated, except in cubic KNT, which shows considerable spectral modifications caused by structural phase transitions and the formation of new OH species in new phases. Although the possible change of the dipole orientation of individual OH vibration with temperatures can be systematically examined by carrying out polarized IR experiments similar to those of Zhang et al. (2001) under in situ conditions, it is beyond the main objective of the present investigation.

Acknowledgments

M.Z. acknowledges support form the Royal Society through the China-UK Science Network Scheme. G.A.L. is grateful to support by the National Science Foundation through grant EAR-0337534. J.Y.W. acknowledges financial support by State 973 program of China (2004CB619002). L.W. is grateful for financial support from the National Natural Science Foundation of China (40472028). The manuscript benefited from reviews and comments by George R. Rossman, Vicky Hamilton, and an anonymous reviewer, and comments from the associate editor, Brigitte Wopenka.

References cited

Agranat, A., Leyva, V., and Yariv, A. (1989) Voltage-controlled photorefractive effect in paraelectric $KTa_{1-x}Nb_xO_3$: Cu, V. Optical Letter, 14, 1017–1019.

Aines, R.D. and Rossman, G.R. (1984) Water in minerals? A peak in the infrared. Journal of Geophysical Research, 89, 4059–4071.

——— (1985) The high temperature behavior of trace hydrous components in silicate minerals. American Mineralogist, 70, 1169–1179.

Bailey, E.B. (1966) The status of clay mineral structures. Clays and Clay Minerals, 26, 1–23.

Bailey, S.W. (1988) Hydrous phyllosilicates (Exclusive of Micas), 19. Reviews in Mineralogy, Mineralogical Society of America, Chantilly, Virginia.

Behrens, H., Romano, C., Nowak, M., Holtz, F., and Dingwell, D.B. (1996) Near-infrared spectroscopic determination of water species in glasses of the system $MAlSi_3O_8$ (M = Li, Na, K): an interlaboratory study. Chemical Geology, 128, 41–63.

Bendow, B. (1973) Frequency and temperature dependence of anharmonicity-induced multiphonon absorption. Physics Review B, 8, 5821–5827.

Bendow, B., Ying, S.C., and Yukon, S.P. (1973) Theory of multiphonon absorption due to anharmonicity in crystals. Physics Review B, 8, 1679–1689.

Bendow, B., Yukon, S.P., and Ying, S.C. (1974) Theory of multiphonon absorption due to nonlinear electric moments in crystals. Physics Review B, 10, 2286–2299.

Bendow, B., Lipson, H.G., and Yukon, S.P. (1977) Multiphonon absorption in highly transparent semi onducting crystals. Physics Review B, 16, 2684–2693.

Bendow, B., Lipson, H.G., and Mitra, S.S (1978) Low-temperature studies of multiphonon absorption in $MgF_2$and $KMgF_3$. Bulletin of the American Physical Society, 23, 342–342.

Bendow, B., Lipson, H.G., Brown, R.N., Marshall, R.C., Billard, D., and Mitra, S.S. (1981) Temperature-dependence of multiphonon absorption in highly transparent cubic zirconia. Journal de Physique, 42, 140–142.

Beran, A. (1970) Messung des Ultrarot-Pleochroismus von Mineralen. IX Der Pleochroismus der OH-Streckfrequenz in Titanit. Tschermaks Mineralogische und Petrographische Mitteilungen, 14, 1–5.

Birman, J.L. (1963) Theory of infrared and Raman processes in crystals: selection rules in diamond and zincblende. Physics Review, 131, 1489–1496.

Bolkenhtein, M.B., Gribov, L.A., Eliashevich, M.A., and Stepanov, B.I. (1972) Molecular Vibrations. Nauka, Moscow.

Born, M. and Huang, K. (1968) Dynamical theory of crystal lattices. Oxford University Press, London.

Boyer, L.L., Harrington, J.A., Hass, M., and Rosenstock, H.B. (1975) Multiphonon absorption in ionic crystals. Physical Review B, 11, 1665–1680.

Brüesh, P. (1986) Phonons: Theory and Experiments. II Experiments and Interpretation of Experimental Results. Springer-Verlag, Berlin.

Carroll, M.R. and Blank, J.G. (1997) The solubility of H_2O in phonolitic melts. American Mineralogist, 82, 549–556.

Cowley, R.A. (1963) The lattice dynamics of an anharmonic crystal. Advances in Physics, 12, 412–480.

Dahm, S. and Risnes, S (1999) A comparative infrared spectroscopic study of hydroxide and carbonate absorption bands in spectra of shark enameliod, shark dentin, and a geological apatite. Calcified Tissue International, 65, 459–465.

Davies, P.R. and Orville-Thomas, W.J. (1969) Infrared band intensities and bond polarities. Part I. Bond moments constants in CO_2, OCS, CS_2, CSe_2, and SCSe. Journal of Molecular Structure, 4, 163–177.

Davydov, A.S. (1976) Quantum mechanics, 2nd edition. Pergamon Press, Oxford.

Decius, J.C. and Hexter, R.M. (1977) Molecular Vibrations in Crystals. McGraw-Hill, New York.

Deer, W.A., Howie, R.A., and Zussman, J. (1992) An introduction to the rock-forming minerals, 2nd edition. Longman Scientific and Technical, London.

Deutsch, T.F. (1974) The 10.6-μm absorption of KCl. Applied Physics Letters, 25, 109–112.

Elliott, J.C. (1994) Structure and chemistry of the apatites and other calcium orthophosphates. Elsevier, Amsterdam.

Engstrom, H., Bates, J.B., and Boatner, L.A. (1980) Infrared spectra of hydrogen isotopes in potassium tantalite. Journal of Chemical Physics, 73, 1073–1077.

Fei,Y. (1995) Thermal expansion in A Handbook of Physical Constants: Mineral Physics and Crystallography. AGU Reference Shelf 2, American Geophysical Union, 29–44.

Fray, S.J., Johnson, F.A., and Jones, R. (1960) Lattice Absorption Bands in Indium Antimonide. Proceedings of the Physical Society of London, 76, 939–948.

Galabov, B. and Orville-Thomas, W.J. (1973) Infrared band intensities and bond polarities: Part 4. The bond-bending vibration of acetylene. Journal of Molecular Structure, 18, 169–176.

Garbuny, M. (1965) Optical Physics. Academic Press Inc, New York.

Guggenheim, M., Chang, Y.H., and Koster van Groos, A.F. (1987) Muscovite dehydroxylation: High-temperature studies. American Mineralogist, 72, 537–550.

Hammer, V.M.F., Beran, A., Endisch, D., and Rauch, F. (1996) OH concentrations in natural titanites determined by FTIR spectroscopy and nuclear-reaction analysis. European Journal of Mineralogy, 8, 281–288.

Hardy, J.R. and Agrawal, B.S. (1973) Determination of the origin of the 10.6-μm absorption in CO_2 laser window materials. Applied Physics Letters, 22, 236–237.

Harrington, J.A. and Hass, M. (1973) Temperature dependence of multiphonon

absorption. Physical Review Letters, 31, 710–713.
Hemley, R.J., Jephcoat, A.P., Mao, H.K., Zha, C.S., Finger, L.W., and Cox, D.E. (1987) Static compression of H_2O-ice to 128 GPa (1.28 Mbar). Nature, 330, 737–740.
Hofmeister, A.M., Cynn, H., Burnley, P.C., and Meade, C. (1999) Vibrational spectroscopy of dense, hydrous magnesium silicates at high pressure: Importance of the hydrogen bond angle. American Mineralogist, 84, 454–464.
Hollas, J.M. (1996) Modern Spectroscopy, 3rd edition. Wiley, New York.
Ihinger, P.D., Zhang, Y., and Stolper, E.M. (1999) The speciation of dissolved water in rhyolitic melt. Geochimica et Cosmochimica Acta, 63, 3567–3578.
Imai, T., Yagi, S., and Yamazaki, H. (1996) Thermal fixing of photorefractive holograms in $KTa_{1-x}Nb_xO_3$ and its relation to proton concentration. Journal of Optical Society of American, B13, 2524–2529.
Isetti, G. and Penco, A.M. (1968) La posizione dell'Idrogeno ossidrilico nella titanite. Mineralogica et Petrographica Acta, 14, 115–122.
Johnson, E.A. and Rossman, G.R. (2003) The concentration and speciation of hydrogen in feldspars using FTIR and ^{1}H MAS NMR spectroscopy. American Mineralogist, 88, 901–911.
Keppler, H. and Bagdassarov, N.S. (1993) High-temperature FTIR spectra of H_2O in rhyolite melt to 1300 °C. American Mineralogist, 78, 1324–1327.
Keppler, H. and Rauch, M. (2000) Water solubility in normally anhydrous minerals measured by FTIR and ^{1}H MAS NMR: the effect of sample preparation. Physics and Chemistry of Minerals, 27, 371–376.
Kleinman, D.A. (1960) Anharmonic forces in the GaP crystal. Physical Review, 118, 118–127.
Knittle, E., Jeanloz, R., and Smith, G.L. (1986) Thermal expansion of silicate perovskite and stratification of the Earth's mantle. Nature, 319, 214–216.
Kolesov, B. and Geiger, C. (2005) The vibrational spectrum of synthetic hydrogrossular (katoite) $Ca_3Al_2(O_4H_4)_3$: A low temperature IR and Raman spectroscopic study. American Mineralogist, 90, 1335–1341.
Kramers, H.A. (1926) Some remarks on the theory of absorption and refraction of X-rays. Nature, 117, 775–778.
Kronig, R.deL. (1926) The theory of dispersion of X-rays. Journal of the Optical Society of America, 12, 547–557.
Kunz, M., Arlt, T., and Stolz, J. (2000) In situ powder diffraction study of titanite ($CaTiOSiO_4$) at high pressure and high temperature. American Mineralogist, 85, 1465–1473.
Lager, G.A., Ambruster, T., and Faber, J. (1987) Neutron and X-ray diffraction study of hydro garnet $Ca_3Al_2(O_4H_4)_3$. American Mineralogist, 72, 756–765.
Lager, G.A., Marshall, W.G., Liu, Z., and Towns, R. (2005) Re-examination of the hydrogarnet structure at high pressure using powder diffraction and infrared spectroscopy. American Mineralogist, 90, 639–644.
Langer, K., Robarick, E., Sobolev, N.V., Shatsky, V.S., and Wang, W. (1993) Single-crystal spectra of garnet from dismondiferous high-pressure metamorphic rocks from Kazakhstan: implication for OH^-, H_2O and FeTi charge transfer. European Journal of Mineralogy, 5, 1091–1100.
Lax, M. and Burstein, E. (1955) Infrared lattice absorption in ionic and homopolar crystals. Physics Review, 97, 39–52.
Levitt, S.R. and Condrate, R.A. (1970) The polarised infrared spectra of hydroxyl ion in fluorapatite. Applied Spectroscopy, 24, 288–289.
Li, H.H. (1980) The infrared absorption coefficient of alkali halides. International Journal of Thermophysics, 1, 97–134.
Libowitzky, E. and Beran, A. (2004) IR spectroscopic characterisation of hydrous species in minerals. In A. Beran and E. Libowitzky, Eds., Spectroscopic methods in mineralogy, 6, p. 227–279. EMU Notes in Mineralogy, Eoetvoes University Press, Budapest.
Libowitzky, E. and Rossman, G.R. (1997) An IR absorption calibration for water in minerals. American Mineralogist, 82, 1111–1115.
Lipson, H.G., Bendow, B., Massa, N.E., and Mitra, S.S. (1976) Multiphonon infrared absorption in the transparent regime of alkaline-earth fluorides. Physical Review B, 13, 2614–2519.
Liu, Y., Behrens, H., and Zhang, Y. (2004) The speciation of dissolved H_2O in dacitic melt. American Mineralogist, 89, 277–284.
Malinin, D.R. and Yoe, J.H. (1961) Development of the laws of colorimetry. Journal of Chemical Education, 38, 129–131.
Maradudin, A.A. and Mills, D.L. (1973) Temperature dependence of the absorption coefficient of alkali halides in the multiphonon Regime. Physical Review Letters, 31, 718–721.
Martin, D.H. (1965) The vibrations of crystal lattices by far-infrared spectroscopy. Advances in Physics, 14, 39–99.
McMillan, P.F. (1995) Water solubility and speciation models. In M.R. Carroll and J.R. Holloway, Eds., Volatiles in Magmas, 30, p. 131–156. Reviews in Mineralogy, Mineralogical Society of America, Chantilly, Virginia.
McNelly, T.F. and Pohl, D.W. (1974) Multiphonon optical spectrum of NaF. Physical Review Letters, 32, 1305–1308.
Meyer, H.W., Zhang, M., Bismayer, U., Salje, E.K.H., Schmidt, C., Kek, S., Morgenroth, W., and Bleser, T. (1996) Phase transformation of natural titanite: An infrared, Raman spectroscopic, optical birefringence and X-ray diffraction study. Phase Transitions, 59, 39–60.
Miles, P.A. (1977) Temperature dependence of multiphonon absorption in zinc selenide. Applied Optics, 16, 2891–2896.
Mills, D.L. and Maradudin, A.A. (1973) Theory of infrared absorption by crystals in the high-frequency wing of their fundamental lattice absorption. Physics Reviews B, 8, 1617–1630.
Mottana, A., Sassi, F.P., Thompson, Jr., J.B, and Guggenheim, S., Eds. (2002) Micas: Crystal chemistry and metamorphic petrology, 46. Reviews in Mineralogy and Geochemistry, Mineralogical Society of America, Chantilly, Virginia.
Nakamoto, K., Margoshes, M., and Rundlt, R.E. (1955) Stretching frequencies as a function of distances in hydrogen bonds. Journal of the American Chemical Society, 77, 6480–6486.
Namjoshi, K.V. and Mitra, S.S. (1974) Infrared-absorption by alkali-halides in transparent regime and its temperature-dependence. Solid State Communications, 15, 317–320.
Nedoluha, A. (1970) Selection rules for anharmonic interactions of nearest neighbors in crystals with the zinc blende or diamond structure. Physics Reviews B, 1, 864–875.
Novak, A. (1974) Hydrogen bonding in solids. Correction of spectroscopic and crystallographic data. Structure and Bonding, 18, 177–216.
Nowak, M. and Behrens, H. (1995) The speciation of water in haplogranitic glasses and melts determined by in situ near-infrared spectroscopy. Geochimica et Cosmochimica Acta, 59, 3445–3450.
Okumura, S. and Nakashima, S. (2005) Molar absorptivities of OH and H_2O in rhyolitic glass at room temperature and at 400–600 °C. American Mineralogist, 90, 441–447.
Okumura, S., Nakamura, M., and Nakashima, S. (2003) Determination of molar absorptivity of IR fundamental OH-stretching vibration in rhyolitic glasses. American Mineralogist, 88, 1657–1662.
Paterson, M.S. (1982) The determination of hydroxyl by infrared absorption in quartz, silicate glasses and similar materials. Bulletin de Minéralogie, 105, 20–29.
Pei, F.M. and Shi, Y. (1996) Geological characteristics of the sericite deposits in Xiling, Song County and preliminary analysis of its genesis. Henan Geology, 14, 160–167 (in Chinese).
Petit, S., Martin, F., Wieqiora, A., de Parseval, P., and Decarreau, A. (2004) Crystal-chemistry of talc: A near infrared (NIR) spectroscopy study. American Mineralogist, 89, 319–326.
Pfeiffer, H.G. and Liebhafsky, H.A. (1951) The origins of Beer's Law. Journal of Chemical Education, 28, 123–125.
Piccirillo, C., Davies, G., Mainwood, A., Scarle, S., and Penchina, C.M. (2002) Temperature dependence of intrinsic infrared absorption in natural and chemical-vapor deposited diamond. Journal of Applied Physics, 92, 756–763.
Rayner, J.H. and Brown, G. (1966) Structure of pyrophyllite. Clays and Clay Minerals, 25, 73-84.
Rosenstock, H.B. (1973) Multiphonon absorption by ionic crystals: Temperature dependence. Journal of Applied Physics, 44, 4473–4477.
——— (1974) Multiphonon absorption in alkali halides: Quantum treatment of Morse potential. Physical Review B, 9, 1963–1970.
Rossman, G.R. (1988) Vibrational spectroscopy of hydrous components. In F.C. Hawthorne, Ed., Spectroscopic Methods in Mineralogy and Geology, 18, p. 193–206. Reviews in Mineralogy, Mineralogical Society of America, Chantilly, Virginia.
Rossman, G.R. and Aines, R.D. (1991) The hydrous components in garnets: Grossular-hydrogrossular. American Mineralogist, 76, 1153–1164.
Rothbauer, R. (1971) Untersuchung eines $2M_1$-Muskovits mit Neutronenstrahlen. Neues Jahrbuch für Mineralogie Monatshefte, 143–154.
Rowe, J.M. and Harrington, J.A. (1976) Temperature dependence of surface and bulk absorption in NaCl and KCl at 10.6 μm. Physical Review B, 14, 5442–5450.
Russell, J.D., Farmer, V.C., and Velde, B. (1970) Replacement of OH by OD in layer silicates and identification of the vibrations of these groups in infrared spectra. Mineralogical Magazine, 37, 869–879.
Salje, E.K.H., Zhang, M., and Groat, L.A. (2000) Dehydration and recrystallization of metamict titanite under thermal anneal: an IR spectroscopic study. Phase Transitions, 71, 173–187.
Sata, N., Hiramoto, K., Ishigame, M., Hosoya, S., Niimura, N., and Shin, S. (1996) Site identification of protons in $SrTiO_3$: Mechanism for large protonic conduction. Physical Review B, 54, 15795–15799.
Savitzky, A. and Golay, M.J.E. (1964) Smoothing and differentiation of data by simplified least squares procedures. Analytical Chemistry, 36, 1627–1639
Schall, M., Walther, M., and Jepsen P.U. (2001) Fundamental and second-order phonon processes in CdTe and ZnTe. Physical Review B, 64, 094301.
Schnepp, O. (1967) Theory for the infrared absorption intensities of the lattice vibrations of molecular solids. Journal of Chemical Physics, 46, 3983–3990.
Shen, A. and Keppler, H. (1995) Infrared spectroscopy of hydrous silicate melts to 1000 °C and 10 Kbar: direct observation of H_2O speciation in a diamond anvil cell. American Mineralogist, 80, 1335–1338.
Sherwood, P.M.A. (1972) Vibrational Spectroscopy of Solids. Cambridge University Press, U.K.

Shi, J., Klocke, A., Zhang, M., and Bismayer, U. (2003) Thermal behavior of dental enamel and geologic apatite: an infrared spectroscopic study. American Mineralogist, 88, 1866–1871.

Sowerby, J. and Keppler, H. (1999) Water speciation in rhyolitic melt determined by in-situ infrared spectroscopy. American Mineralogist, 84, 1843–1849.

Sparks, M. (1973) Temperature and frequency dependence of infrared absorption as a diagnostic tool. Applied Physics Letters, 23, 368–369.

——— (1974) Infrared absorption by the higher-order-dipole-moment mechanism. Physical Review B, 10, 2581–2589.

Sparks, M. and Sham, L.J. (1972) Exponential frequency dependence of multiphonon-summation infrared absorption. Solid State Communications, 11, 1451–1456.

——— (1973a) Temperature dependence of multiphonon infrared absorption. Physical Review Letters, 31, 714–717.

——— (1973b) Theory of multiphonon absorption in insulating crystals. Physical Review B, 8, 3037–3048.

Speer, J.A. and Gibbs, G.V. (1976) The crystal structure of synthetic titanite, $CaTiOSiO_4$, and the domain textures of natural titanites. American Mineralogist, 61, 238–247.

Stoeckli-Evans, H. Barnes, A.J., and Orville-Thomas, W.J. (1975) Infrared band intensities and bond polarities: Part 5—XCl_4 molecules (X = C, Si, Ge, Sn). Journal of Molecular Structure, 24, 73–83.

Stolper, E.M. (1982) Water in silicate glasses: an infrared spectroscopic study. Contributions to Mineralogy and Petrology, 81, 1–17.

Struzhkin, V.V, Goncharov, A.F, Hemley, R.J., and Mao, H-K. (1997) Cascading Fermi Resonances and the Soft Mode in Dense Ice. Physical Review Letters, 78, 4446–4449.

Taylor, M. and Brown, G.E. (1976) High-temperature structural study of the $P2_1/a \Leftrightarrow A2/a$ phase transition in synthetic titanite, $CaTiSiO_5$. American Mineralogist, 61, 435–447.

Thibaudeau, P., Debeernardi, A., Phuoc, V.T., Rocha, S.D., and Gervais, F. (2006) Phonon anharmonicity in disordered $MgAl_2O_4$ spinel. Physical Review B, 73, 064305.

Thomas, G.A., Ladd, J.A., and Orville-Thomas, W.J. (1969) Infrared band intensities and bond polarities: Part 2. Bond moment constants in linear triatomic molecules using zero-order bond moment theory. Journal of Molecular Structure, 4, 179–190.

Thomas, G.A., Jalsovszky, G., Ladd, J.A., and Orville-Thomas, W.J. (1971) Infrared band intensities and bond polarities: Part 3. Bond moment constants in linear triatomic molecules using first-order bond moment theory. Journal of Molecular Structure, 8, 1–9.

van Straten, A.J. and Smit, W.M.A. (1976) Bond charge parameters from integrated infrared intensities. Journal of Molecular Spectroscopy, 62, 297–312.

Wang, J.Y., Guan, Q.C., Wei, J.Q., Wang, M., and Liu, Y.G. (1992a) Growth and characterization of cubic $KTa_{1-x}Nb_xO_3$ crystals. Journal of Crystal Growth, 116, 27–36.

Wang, L., Zhang, M., Redfern, S.A.T., and Zhang, Z.Y. (2002) Dehydroxylation and transformations of the 2:1 phyllosilicate pyrophyllite at elevated temperatures: An infrared spectroscopic study. Clays and Clay Minerals, 50, 272–283.

Wang, L., Zhang, M., and Redfern, S.A.T. (2003) Infrared study of CO_2 incorporation into pyrophyllite $[Al_2Si_4O_{10}(OH)_2]$ during dehydroxylation. Clays and Clay Minerals, 51, 439–444.

Wang, M., Yang, Z.H., Wang, J.Y., Liu, Y.G., Guan, Q.C., and Wei, J.Q. (1992b) The thermal-properties of $KTa_{1-x}Nb_xO_3$ crystal. Ferroelectrics, 132, 55–60.

Ward, J.R. (1975) Kinetics of talc dehydroxylation. Thermochimica Acta, 13, 7–14.

Wardle, R. and Brindley, G.W. (1972) The crystal structures of pyrophyllite, 1Tc, and of its dehydroxylate. American Mineralogist, 57, 732–750.

Weber, G., Kapphan, S., and Wöhlecke, M. (1986) Spectroscopy of the O-H and O-D stretching vibrations in $SrTiO_3$ under applied electric field and uniaxial stress. Physical Review B, 34, 8406–8417.

Wilkins, R.W.T. and Ito, J. (1967) Infrared spectra of some synthetic talc. American Mineralogist, 52, 1649–1661.

Withers, A.C. and Behrens, H. (1999) Temperature-induced changes in the NIR spectra of hydrous albitic and rhyolitic glasses between 300 and 100 K. Physics and Chemistry of Minerals, 27, 119–132.

Zhang, M., Wruck, B., Graeme-Barber, A. Salje, E.K.H., and Carpenter, M.A. (1996) Phonon spectra of alkali-feldspars: phase transitions and solid solutions. American Mineralogist, 81, 92–104.

Zhang, M., Salje, E.K.H., and Bismayer, U. (1997) Structural phase transition near 825 K in titanite: Evidence from infrared spectroscopic observations. American Mineralogist, 82, 30–35.

Zhang, M., Salje, E.K.H., Malcherek, T., Bismayer, U., and Groat, L.A. (2000) Dehydration of metamict titanite: an infrared spectroscopy study. Canadian Mineralogist, 38, 119–130.

Zhang, M., Groat, L.A., Salje, E.K.H., and Beran, A. (2001) Hydrous species in crystalline and metamict titanites. American Mineralogist, 86, 904-909.

Zhang, M., Wang, L., Hirai, S., Redfern, S.A.T., and Salje, E.K.H. (2005) Dehydroxylation and CO_2 incorporation in annealed mica (sericite): An infrared spectroscopic study. American Mineralogist, 90, 173–180.

Zhang, M., Hui, Q., Lou, J.X., Redfern, S.A.T., Salje, E.K.H., and Tarantino, S.C. (2006) Dehydroxylation, proton migration and structural changes in heated talc: An infrared spectroscopic study. American Mineralogist, 91, 816–825.

Zhang, Y., Stolper, E.M., and Ihinger, P.D. (1995) Kinetics of the reaction $H_2O + O = 2OH$ in rhyolitic and albitic glasses: preliminary results. American Mineralogist, 80, 593–1661.

Zhang, Y., Xu, Z., and Behrens, H. (2000) Hydrous species geospeedometer in rhyolite: improved calibration and applications. Geochimica et Cosmochimica Acta, 64, 3347–3355.

Manuscript received January 31, 2007
Manuscript accepted April 26, 2007
Manuscript handled by Brigitte Wopenka